

# Predictions of conventional and microscopic triaxial cranking models for light nuclei

P. Gulshani

NUTECH Services, 3313 Fenwick Crescent, Mississauga, Ontario, Canada L5L 5N1  
Tel. #: 647-975-8233; matlap@bell.net; ORCID #: 0000-0002-3391-6491

## Abstract

The conventional cranking model (CCRM3) uses a constant angular velocity to study rotational features in deformed nuclei. To investigate the effect of a dynamic angular velocity, a quantal microscopic cranking model for triaxial rotation (MSCRM3) is derived from a unitary transformation of the nuclear Schrodinger equation to a rotating frame and using Hartree-Fock method. Except for a microscopically determined angular velocity and hence time-reversal and  $D_2$  invariance in MSCRM3, MSCRM3 and CCRM3 Schrodinger equations are identical in form, and hence are solved iteratively in a similar manner. The differences between the rotational features predicted by CCRM3 and MSCRM3 are demonstrated in the simplest setting with the fewest number of free parameters by applying CCRM3 and MSCRM3 to  $^{20}\text{Ne}$ ,  $^{24}\text{Mg}$ , and  $^{28}\text{Si}$  and using a self-consistent deformed harmonic-oscillator potential. In the iterative procedure, oscillatory solutions are avoided using linear mixing of input and output conditions. The article investigates, over the possible range of the model parameters and nuclei  $^{20}\text{Ne}$ ,  $^{24}\text{Mg}$ , and  $^{28}\text{Si}$ , rotational relaxation of the intrinsic system and stability of the MSCRM3 and CCRM3 predicted uniform, planar, triaxial, and axially and spherically symmetric rotations and nuclear shapes and their transitions, rotational band termination, and the differences between the two model predictions. The observed reduced energy-level spacing in  $^{20}\text{Ne}$  is explained in terms of wobbly rotation quenching. The impact of spin-orbit and residuals of the square of the angular momentum and quadrupole-quadrupole interaction in  $^{20}\text{Ne}$  is examined. MSCRM3 rules out a free self-sustaining rotation.

*PACS number: 21.60.Ev, 21.60.Fw, 21.60.Jz*

**Keywords:** uniform, planar, wobbly, tilted-axis, triaxial, axially and spherically symmetric rotations; closed-form solution of 3-D cranked deformed-self-consistent-oscillator governing equations; impact of spin-orbit and residual two-body interaction and square of angular momentum; strong coupling of intrinsic and collective-rotational motions; positive intrinsic-rotation feedback mechanism; inherently unstable cranked rotational states; rotational-band termination on axial and spherical symmetry; time-reversal and  $D_2$  invariance; rigid-flow velocity-field prescription; optimally intrinsic rotor Hamiltonian; corrections to the conventional cranking model; rotation relaxation; shape and rotation-mode transitions; wobbly-rotation quenching, reduced yrast energy-level spacing in  $^{20}\text{Ne}$ ; self-sustaining rotation

## 1. Introduction

It can be argued [1, arXiv:1609.04267, arXiv:1610.08337] that a reasonable separation of intrinsic and collective rotational motions as envisioned in the Bohr rotational model [2-6] cannot be achieved from first principles except under extreme

conditions. Therefore, the nuclear shell model and the conventional cranking model combined with the angular momentum projection methods seem to be the most fruitful approaches for the description of the nuclear rotational motion. The conventional

cranking model for collective rotation about a single principal axis is frequently used to investigate the observed nuclear rotational properties (such as rotational bands, Coriolis anti-pairing, angular momentum alignment, back-bending, band termination, etc.) [6-44]. Other nuclear rotational features (such as precession, wobbling, tilted rotation, etc.), which involve a rotation about an arbitrary axis, have been studied [40,45-60] using a straightforward triaxial generalization of the uniaxial cranking model and solving numerically the model Schrodinger equation for a self-consistent potential energy. A number of studies have used the uniaxial [5,6,7,12,13,14,17,18,23,41,42] and triaxial [45-48,51,54] cranking models with a self-consistent deformed harmonic-oscillator potential to predict general rotational properties of nuclei and obtain physical insight in a physically transparent calculation with the least number of adjustable parameters using respectively analytical and numerical solution methods.

It is generally recognized [5,6,61] that the cranking model is phenomenological, semi-classical, and time-reversal and  $D_2$  non-invariant since the three components of the angular-velocity vector in the model are constant free parameters. To correct this model feature and reveal the implicit model assumptions and approximations, there have been many investigations [6 and references therein, 61-89, arXiv:1810.11836, arXiv:1909.07169] to derive a tractable microscopic cranking model from first principles using various methods (such as canonical transformations, angular-momentum constrained Hartree-Fock (HF), time-dependent HF, time-dependent Lagrangian variation, angular momentum projection, generator co-ordinate, RPA, density matrix, etc.) and approximations (such as expansion in powers of angular

momentum operator, large deformation, redundant co-ordinates, using lowest order density matrix, etc.). These analyses were mostly limited to two-dimensional rotation. One of the major difficulties in these derivations has been defining the orientation angles of the deformed nuclear state and accounting for the strong coupling between the rotation and intrinsic motions. This coupling renders the cranked Hamiltonian a complicated function of the angular momentum operator coupled to other (such as shear) and moment of inertia operators. Therefore, to obtain a cranking-type Hamiltonian, one needs to expand the Hamiltonian to second power of the angular momentum and tackle the coupled rotation-intrinsic operators.

In this article, we overcome these difficulties by equating the cranked wavefunction for triaxial rotation to a rotated deformed nuclear wavefunction and choosing the three rotation angles with respect to the space-fixed (and not body-fixed) frame axes to be specified by a rigid-flow velocity-field prescription. This prescription decouples the rotation and intrinsic motions renormalizing the kinematic moment of inertia to the rigid-flow moment, and renders the cranked Hamiltonian dependent only on the square of the angular momentum operators. (Note that the rigid-flow prescription does not constrain the motion of the particles in any way, and hence redundant coordinates are not needed.) The resulting microscopic cranking model for triaxial rotation is dubbed MSCRM3 and the corresponding conventional cranking model is dubbed CCRM3.

This article compares, over the possible range of the model parameters, the rotational features predicted by the conventional (CCRM3) and microscopic (MSCRM3) cranking models for  $^{20}\text{Ne}$ ,  $^{24}\text{Mg}$ , and  $^{28}\text{Si}$ . In Section 2 of this article, we solve in closed forms the coupled CCRM3 equations for a

self-consistent deformed harmonic-oscillator potential energy<sup>1</sup> using Feynman's theorem [90] and the solution of CCRM3 characteristics equation. The angles orienting the angular-velocity vector and the self-consistent oscillator-potential frequencies are determined from the usual minimization of the intrinsic energy with respect to the angles and separately with respect to the oscillator frequencies subject to a constant-volume condition. The resulting coupled CCRM3 closed-form algebraic equations are solved iteratively for a desired value of the angular-momentum quantum number  $J$  by varying the magnitude of the angular-velocity vector to achieve the desired  $J$ .

In Section 3, we derive from first principles a microscopic, self-consistent, time-reversal and  $D_2$  invariant cranking model for triaxial rotation (MSCRM3) in two steps. In the first step, we apply a rotationally-invariant exponential rotation operator to a deformed nuclear state to transform the nuclear Hamiltonian (actually the kinetic energy term in the Hamiltonian as explained in Section 3) into a microscopic optimally-intrinsic rotor Hamiltonian. The rotation invariance of the rotation operator renders the transformed Hamiltonian symmetric in the angular momentum components, in contrast to an asymmetric Hamiltonian form obtained when the Euler angles are used. The three rotation angles in the rotation operator are chosen to describe rotation about each of the three space-fixed (and not body-fixed) axes, and to satisfy a collective rigid-flow velocity-field prescription. This prescription eliminates the need for constraints on the particle co-ordinates, and for redundant co-ordinates used in previous analyses [62,63]. It also eliminates any explicit coupling of the angular-momentum operators to any

intrinsic operators yielding a tractable rotor Hamiltonian that depends only on the square of the angular-momentum operators and on the kinematic rigid-flow moment of inertia. The rotor Hamiltonian obtained thereby is also optimally intrinsic. These features make it unnecessary to use any major approximations and assumptions in the derivation of MSCRM3 and renders the derivation quantum and microscopic and its connection with CCRM3 explicitly transparent. In the second step, we apply HF variational and second quantization methods to the rotor Hamiltonian to derive MSCRM3 Hamiltonian as the mean-field part of the rotor Hamiltonian, supplemented by residual correction terms associated with the square of the angular-momentum operators and two-body nucleon interaction, and negligibly small terms in the product of the quadrupole-moment and angular-momentum operators, and angular velocities. MSCRM3 is a microscopic generalization of CCRM3 and of the Thouless-Valatin semi-classical low-angular-velocity model for uniaxial rotation [61]. The MSCRM3 and CCRM3 Schrodinger equations look identical except that the angular velocity in MSCRM3 is not a free constant parameter but is a quantum microscopic and dynamic variable determined by the microscopic collective rigid-flow velocity-field prescription.

In contrast, previous attempts to derive a microscopic cranking model [6 and references therein, 13, 61-89, arXiv:1609.04267, arXiv:1708.03326, arXiv:1810.11836, arXiv:1909.07169] were mostly limited to rotation in two dimensions and used a significant number of major approximations and assumptions such as large deformation, large expectation of an angular momentum component, expansion in powers of the angular momentum, angular momentum projection, and generator co-

---

<sup>1</sup> We use the simple deformed harmonic oscillator potential to allow us to compare the MSCRM3 predictions with those of CCRM3 in

[5,6,7,12,13,14,17,18,23,41,42,45-48,,51,54], which used this potential.

ordinates method using various simplifying approximations such as axial symmetry, expansion in density matrices and limiting the analysis to single-particle density matrix, constraint and time-dependent HF, (small-amplitude rotation) RPA, etc. In particular, reference [69] assumes a two-dimensional rotation of a well-deformed independent-particle ground state possessing a large value of the expectation of the square of the angular momentum. It assumes that the rotation angle  $\phi''$  is canonically conjugate to the angular momentum operator  $\hat{J}$  and expands the Hamiltonian  $\hat{H}$  in powers of  $\hat{J}$ ,  $\phi''$ , and  $[\hat{H}, \phi'']$ . It then assumes that  $\phi''$  is a function of particle coordinates, and this renders the Hamiltonian to depend on  $\hat{J}$  and  $\hat{J}^2$  where the  $\hat{J}$  term involves a product of  $\hat{J}$  and the particle momenta. This  $\hat{J}$  term represents the coupling between the rotational and intrinsic motions. Reference [69] then minimizes the expectation of  $\hat{H}$  in a particle-hole HF approximation up to

## 2. Derivation of coupled algebraic CCRM3 equations

The objective of this section is to show how to solve the CCRM3 iteratively instead of numerically (i.e., Hamiltonian diagonalization in the phase space), which has been done so far.

To study triaxial rotation, rotational bands, and the excitation energies in triaxial  $^{24}\text{Mg}$ , [45] solved numerically the CCRM3 Schrodinger equation using a deformed harmonic oscillator potential. The analysis in [51,54] also solved numerically the equation of the deformed-harmonic-oscillator CCRM3, and studied the stability of tilted rotation of nuclei over a range of mass numbers. The analysis in [54] concluded that in even-even nuclei tilted rotations occur if and only if the nucleus has a triaxial shape in its ground state. This

second order in  $\hat{J}^2$  to obtain an expression for the effective moment of inertia similar to that of Thouless-Valatin.

Section 4 presents the predictions of CCRM3 and MSCRM3 and discusses the differences between these and previous predictions of CCRM3 in [5,6,7,12,13,14,17,18,23,41,42,45-48,51,54] for the light nuclei  $^{20}\text{Ne}$ ,  $^{24}\text{Mg}$ , and  $^{28}\text{Si}$ . Section 4 also investigates the impact of spin-orbit and residuals of the square of the angular momentum operator and of quadrupole-quadrupole interaction on these predictions.

Section 5 summarizes the model development, predictions, the differences between the two-model predictions, and between these and previous CCRM3 predictions. Section 5 then presents the conclusions.

Appendix A presents the details of the derivation of the microscopic, quantum, intrinsic rotor Hamiltonian described in Section 3.

conclusion is compared with the predictions of CCRM3 in Section 4. Reference [46] used a tilted deformed harmonic-oscillator potential in CCRM3 to show that tilted rotation is unstable. However, the analysis [46] assumed that the off-diagonal frequencies in the tilted potential can be varied independently of the diagonal frequencies. This assumption is not supported by our results in [arXiv:1909.07169, Eqs (42) and (43) page 11], where it is shown that the off-diagonal frequencies are functions of the diagonal frequencies. Nevertheless, the CCRM3 predictions in Section 4 show that not only tilted rotation but all cranked rotational states (with the exception of uniform planar rotations) are unstable unless the rotation is maintained by an external angular momentum constraint as in the conventional

cranking model. Assuming a uniform rotation and using an isotropic harmonic-oscillator potential combined with HF mean-field part of the separable quadrupole-quadrupole two-body interaction, Reference [48] claims to show the existence of a time-dependent HF tilted rotation. This result seems to support the MSCRM3 result in Section 4 that only a planar rotation followed by a transition to a uniform principal-axis rotation can explain the observed yrast-line curvature in  $^{20}\text{Ne}^2$ .

In this section, we reduce the deformed-harmonic-oscillator CCRM3 Schrodinger equation and the self-consistency-constant-volume condition equations to coupled algebraic equations and solve them iteratively as follows<sup>3</sup>. The CCRM3 cranked Hamiltonian is:

$$\begin{aligned}\hat{H}_{cr} &\equiv \hat{H}_o - \vec{\Omega}' \cdot \vec{j} \\ &\equiv \sum_{n=1}^A \hat{h}_{cr}(n) \equiv \sum_{n=1}^A \left[ \hat{h}_o(n) - \vec{\Omega}' \cdot \vec{j}(n) \right] \quad (1)\end{aligned}$$

where  $\hat{h}_o(n)$  and  $\vec{j}(n)$  are respectively the  $n^{\text{th}}$  particle deformed harmonic-oscillator Hamiltonian and angular-momentum vector operator given by<sup>4</sup>:

$$\begin{aligned}\hat{h}_o &\equiv \sum_{k=1}^3 \left( \frac{p_k^2}{2M} + \frac{M}{2} \omega_k^2 x_k^2 \right), \\ \vec{j} &\equiv \vec{x} \times \vec{p}\end{aligned} \quad (2)$$

and  $\vec{\Omega}'$  is the angular velocity vector with the components, magnitude, and orientation given by:

$$\begin{aligned}\vec{\Omega}' &= (\Omega'_1, \Omega'_2, \Omega'_3) \\ &= \Omega' \cdot (\sin \theta' \cdot \cos \phi', \\ &\quad \sin \theta' \cdot \sin \phi', \cos \theta'), \\ \Omega'^2 &\equiv \Omega_1'^2 + \Omega_2'^2 + \Omega_3'^2\end{aligned}$$

(3)

The three normal-mode frequencies  $\alpha_k$

associated with  $\hat{h}_{cr}$  in Eq. (1) can be determined from solving either the quantum (as in [45]) or classical equation of motion. Both methods yield the same  $\alpha_k$ . We choose to determine  $\alpha_k$  from solving the classical, i.e., Newton's, equations of motion for  $\hat{h}_{cr}$  as follows. The time evolution of a particle co-ordinates and momenta for the cranked Hamiltonian  $\hat{h}_{cr}$  is given in the Heisenberg representation by:

$$\vec{x}(t) = e^{i\hat{h}_{cr}t/\hbar} \vec{x} e^{-i\hat{h}_{cr}t/\hbar} \quad (4)$$

<sup>2</sup> There have been also analyses of the conventional cranking model for triaxial rotation and tilted and wobbly rotation using more realistic potentials including two-body interactions [30,48,52,56,57,91-94].

<sup>3</sup> It is much easier and more transparent to use this approach than to numerically diagonalize the Hamiltonian matrix obtained from Eq. (1) in the phase space [95] coupled to the self-consistency-constant-volume equations as done in [54].

<sup>4</sup> We have not included the  $\vec{l} \cdot \vec{s}$  and  $l^2$  interaction terms from the Nilsson's model in  $\hat{h}_o$  because the  $l^2$  term is negligibly small for  $sd$ -shell nuclei [6 (pages 133,137), 7 (page 217), and 21] . As we show in Section

4, the  $\vec{l} \cdot \vec{s}$  term increases the excitation energy by about 10%. The reordering of the single-particle energy levels produced by  $\vec{l} \cdot \vec{s}$  affects the nuclear deformation.

However, since the main objective in this article is not to compare the predicted results with the experimental results but rather to show the differences (as a consequence of the microscopic angular velocity in MSCRM3) between MSCRM3 and CCRM3 predictions and the previous CCRM3 predictions in [5,6,7,12,13,14,17,18,23,41,42, 45-48,51,54] where  $l^2$  or  $\vec{l} \cdot \vec{s}$  were not used, we can therefore neglect  $l^2$  and  $\vec{l} \cdot \vec{s}$  terms.

Substituting Eqs. (1) and (2) into Eq. (4) and taking first and second time derivatives of  $\vec{x}$ , we obtain the particle acceleration or Newton's equations of motion:

$$M \frac{d^2}{dt^2} x_k(t) = -M \omega_k^2 x_k(t) - 2M \left( \vec{\Omega}' \times \frac{d}{dt} \vec{x}(t) \right)_k - M \left( \vec{\Omega}' \times (\vec{\Omega}' \times \vec{x}(t)) \right)_k \quad (5)$$

A periodic solution in the form

$$\vec{x}(t) = \vec{x}_o \cdot e^{i\alpha t}$$

of the three coupled Eqs. (5) gives three coupled algebraic equations for  $\vec{x}_o$ . These three equations have non-trivial solutions if the following cubic characteristic equation is satisfied:

$$\alpha^6 - A_o \alpha^4 + B_o \alpha^2 - C_o = 0 \quad (6)$$

where (Eq. (6) is identical to that in [45] obtained from solving the quantum equations of motion):

$$\begin{aligned} A_o &\equiv \sum_{k=1}^3 (\omega_k^2 + 2\Omega_k'^2), \\ B_o &\equiv \sum_{k \neq l=1}^3 (\omega_k^2 \omega_l^2 - \omega_k^2 \Omega_l'^2) \\ &\quad + 2 \sum_{k=1}^3 \omega_k^2 \Omega_k'^2 + \left( \sum_{k=1}^3 \Omega_k'^2 \right)^2 \\ C_o &\equiv \omega_1^2 \omega_2^2 \omega_3^2 - \omega_1^2 \omega_2^2 \Omega_1'^2 - \omega_1^2 \omega_3^2 \Omega_1'^2 \\ &\quad - \omega_2^2 \omega_3^2 \Omega_2'^2 - \omega_2^2 \omega_3^2 \Omega_3'^2 - \omega_1^2 \omega_2^2 \Omega_2'^2 \\ &\quad - \omega_1^2 \omega_3^2 \Omega_3'^2 + \omega_2^2 \Omega_1'^2 \Omega_2'^2 + \omega_1^2 \Omega_1'^2 \Omega_3'^2 \\ &\quad + \omega_3^2 \Omega_1'^2 \Omega_3'^2 + \omega_2^2 \Omega_2'^2 \Omega_3'^2 + \omega_1^2 \Omega_1'^2 \Omega_2'^2 \\ &\quad + \omega_3^2 \Omega_2'^2 \Omega_3'^2 + \sum_{k=1}^3 \omega_k^2 \Omega_k'^4 \end{aligned} \quad (7)$$

The three roots of Eq. (6) are the normal-mode frequencies  $\alpha_k$  of  $\hat{H}_{cr}$ , which are readily obtained in closed forms, as functions of  $A_o$ ,  $B_o$ , and  $C_o$ , from the literature.

The intrinsic energy is then given by:

$$\begin{aligned} E_{\text{int}} &\equiv \langle H_{cr} \rangle \equiv \langle H_o - \vec{\Omega}' \cdot \vec{J} \rangle \\ &= \hbar \sum_{k=1}^3 \alpha_k \Sigma_k, \end{aligned} \quad (9)$$

$$\Sigma_k \equiv \sum_{n=1}^{n_{fk}} (n_k + 1)$$

where  $\langle \hat{H}_{cr} \rangle \equiv \langle | \hat{H}_{cr} | \rangle$ ,  $| \rangle$  is a CCRM3 ground-state rotational-band eigenfunction,  $\Sigma_k$  is the ground-state nucleon oscillator-shell total phonon occupation number along the  $k$  axis, and  $n_{kf}$  is the number of oscillator quanta along the  $k$  axis at the Fermi surface.

We then use Eqs. (1), (2), (6) to (9) and the Feynman's theorem [6,14,89] to derive closed-form algebraic expressions for the following expectations with respect to  $| \rangle$  of the CCRM3 operators:

$$\begin{aligned} \langle \hat{J}_k \rangle &= -\frac{\partial E_{\text{int}}}{\partial \Omega_k'} = -\hbar \sum_{l=1}^3 \frac{\partial \alpha_l}{\partial \Omega_k'} \Sigma_l, \\ \frac{M}{2} \langle x_k^2 \rangle &= \frac{\partial E_{\text{int}}}{\partial \omega_k^2} = \hbar \sum_{l=1}^3 \frac{\partial \alpha_l}{\partial \omega_k^2} \Sigma_l \end{aligned} \quad (10)$$

Eqs. (10) must also satisfy the constant nuclear-volume and the density-potential-shapes self-consistency conditions. As is normally done, these conditions imply, in the HF mean-field sense, a minimization of  $E_{\text{int}}$  with respect to the oscillator frequencies  $\omega_k^2$ , yielding the results:

$$\begin{aligned} \omega_1^2 \langle x^2 \rangle &= \omega_2^2 \langle y^2 \rangle = \omega_3^2 \langle z^2 \rangle, \\ \omega_1 \omega_2 \omega_3 &= \omega_o^3 \end{aligned} \quad (11)$$

where  $\omega_o$  is the isotropic nuclear harmonic-oscillator frequency:  $\hbar \omega_o \equiv P A^{-1/3}$  with  $P=35.43$  for light nuclei and  $P=41$  for heavy nuclei.

$\vec{\Omega}'$  in Eq. (3) is determined in the usual manner as follows. The angles  $(\theta', \phi')$  are

chosen to minimize the intrinsic energy  $E_{\text{int}}$ , whence we obtain:

$$\begin{aligned}\tan \phi' &= \langle \hat{J}_2 \rangle / \langle \hat{J}_1 \rangle, \\ \tan \theta' &= \langle \hat{J}_1 \rangle \cdot \sqrt{1 + \tan^2 \phi'} / \langle \hat{J}_3 \rangle\end{aligned}\quad (12)$$

The magnitude  $\Omega'$  of  $\vec{\Omega}'$  is adjusted to satisfy the condition that the wavefunction  $|\rangle$  yields a desired value of  $\langle \hat{J}^2 \rangle$  for a given value of the angular-momentum quantum number  $J$  according to the prescription:

$$\begin{aligned}\langle \hat{J}^2 \rangle &= \langle \hat{J}_1 \rangle^2 + \langle \hat{J}_2 \rangle^2 + \langle \hat{J}_3 \rangle^2 \\ &= \hbar^2 J(J+1)\end{aligned}\quad (13)$$

*for a triaxial rotation*

$$\begin{aligned}\langle \hat{J}^2 \rangle &= \langle \hat{J}_1 \rangle^2 + \langle \hat{J}_2 \rangle^2 + \langle \hat{J}_3 \rangle^2 \\ &= \hbar^2 J^2\end{aligned}\quad (14)$$

*for a principal-axis rotation*

For principal-axis or uniform rotation in Eq. (14), all but one of the angular

### 3. Derivation of MSCRM3

In this section, we derive the microscopic, quantum, self-consistent, time-reversal and  $D_2$  invariant cranking model for triaxial rotation (MSCRM3) and residual corrections to it. We start from the nuclear Schrodinger equation:

$$\begin{aligned}\hat{H}'_o |\Phi\rangle &\equiv \left( \sum_{n=1}^A \frac{\hat{p}_n^2}{2M} + \hat{V} \right) |\Phi\rangle \\ &= E_J |\Phi\rangle\end{aligned}\quad (16)$$

$\hat{V}$  is a rotationally invariant. For open-shell nuclei, we assume that the wavefunction  $|\Phi\rangle$  describes a deformed nucleon spatial configuration or distribution. The assumption is justified based on numerous HF variational calculations that indicate that the mean-field potential energy  $\hat{V}_{\text{HF}}$  is

momentum components are zero and the non-zero component lies along the principal axis similarly to the quantization:  $\hat{J}_3 = m\hbar$  where  $m$  ranges over  $-J, -J+1, \dots, 0, +1, +2, \dots, J$  (but note that we are concerned with the expectation of  $\hat{J}_k$ , which can have any value  $\leq J$ ). We observe that, for the same  $J$  value, the  $\langle \hat{J}^2 \rangle$  value obtained from Eq. (13) is larger than that from Eq. (14), and hence so are the corresponding excitation energies.

The rotational-band excited-state ( $E_J$ ) and excitation ( $\Delta E_J$ ) energies are then determined from:

$$\begin{aligned}E_J &\equiv \langle \hat{H}_o \rangle \equiv \langle \hat{H}_{cr} + \vec{\Omega}' \cdot \vec{\hat{J}} \rangle \\ &= E_{\text{int}} + \vec{\Omega}' \cdot \langle \vec{\hat{J}} \rangle,\end{aligned}\quad (15)$$

$$\Delta E_J \equiv E_J - E_{J=0}$$

anisotropic for nuclei where the nucleons do not fill the single-particle shell at the Fermi level, i.e., they are open-shell nuclei. This scenario is still valid when the residual interaction  $\hat{V}_{\text{res}} \equiv \hat{V} - \hat{V}_{\text{HF}}$  is accounted for in a Tamm-Dancoff or RPA approximation at least when the  $\hat{V}_{\text{res}}$  is not too large.

Therefore, in Eq. (16), we can assume that  $|\Phi\rangle$  describes a deformed ground (no hole states below the Fermi level) or excited (some particles are excited above the Fermi level) state.

We then derive MSCRM3 in two steps. In the first step, we apply the rotationally-invariant exponential rotation operator  $e^{i\vec{\theta} \cdot \vec{\hat{J}}/\hbar}$  to the deformed state  $|\Phi\rangle$  to obtain the rotated state:

$$|\Phi(\theta_k^*)\rangle = e^{i\vec{\theta} \cdot \vec{\hat{J}}/\hbar} |\Phi\rangle \quad (17)$$

Inserting Eq. (17) for  $|\Phi\rangle$  into Eq. (16), we obtain the following microscopic, quantum, rotationally invariant, optimally-intrinsic rotor Schrodinger equation for triaxial rotation (refer to Appendix A for details):

$$\begin{aligned} & \hat{H} |\Phi(\bar{\theta}'')\rangle \\ & \equiv e^{i\bar{\theta}'' \cdot \hat{J}/\hbar} \cdot \hat{H}'_o \cdot e^{-i\bar{\theta}'' \cdot \hat{J}/\hbar} \cdot |\Phi(\bar{\theta}'')\rangle \\ & = \left( \hat{H}'_o - \sum_{l \neq k=1}^3 \frac{\hat{J}_k^2}{2M \hat{\mathcal{J}}_k} \right. \\ & \quad \left. - \sum_{l \neq k=1}^3 \frac{\hat{Q}_{lk}}{2M \hat{\mathcal{J}}_l \hat{\mathcal{J}}_k} \cdot \hat{J}_l \cdot \hat{J}_k \right) |\Phi(\bar{\theta}'')\rangle \\ & = E_J |\Phi(\bar{\theta}'')\rangle \end{aligned} \quad (18)$$

where  $\hat{H}'_o$  is defined in Eq. (16) in view of the rotational invariance of  $\hat{V}$ ,

$\hat{Q}_{lk} \equiv \sum_{n=1}^A x_{nl} \cdot x_{nk}$  is a component of the quadrupole-moment tensor, and  $\hat{\mathcal{J}}_k$  is a principal-axis component of the rigid-flow kinematic moment of inertia tensor operator defined below in Eq. (21). Each of the operator components appearing in Eq. (18), and in the equations to follow, are along space-fixed (and not body-fixed) coordinate-system axes. We obtain the Hamiltonian  $\hat{H}$  in Eq. (18) only when we use the following collective rigid-flow velocity-field prescription for the three rotation angles  $\theta''_k$ :

$$\begin{aligned} \frac{\partial \theta''_l}{\partial x_{nj}} &= - \sum_{k=1 \neq j \neq l}^3 {}_l\chi_{jk} x_{nk}, \\ {}_l\chi_{jk} &= -{}_l\chi_{kj} = 0 \quad \text{for } j, k = l \\ & \quad (l, j, k = 1, 2, 3) \end{aligned} \quad (19)$$

where each of the three  $3 \times 3$  matrices  ${}_l\chi$  is real and anti-symmetric. Each of the three equations in Eq. (19) adds a collective rigid-flow component to each nucleon velocity field. The prescription in Eq. (19) renders Eq. (18) dependent on only  $\hat{J}_k^2$ <sup>5</sup>. The non-zero elements of the matrices  ${}_k\chi$  are determined by choosing  $\theta''_k$  and  $\hat{J}_k$  to be a canonically conjugate pair, which together with Eq. (19) yields:

$$\begin{aligned} {}_l\chi_{jk} &= \frac{1}{\hat{\mathcal{J}}_l}, \quad \hat{\mathcal{J}}_l \equiv \sum_{n=1}^A (x_{nj}^2 + x_{nk}^2), \\ j, k, l &= 1, 2, 3 \quad \text{and in cyclic order} \end{aligned} \quad (20)$$

where  $A$  is the mass number and  $M \hat{\mathcal{J}}_l$  is the  $l^{\text{th}}$  principal-axis component of the rigid-flow moment of inertia tensor in the space-fixed frame.

Eq. (18) shows that, for each  $\theta''_k$  in Eqs. (17) and (18), the rotated deformed wavefunction  $|\Phi(\theta''_k)\rangle$  corresponds to the same energy  $E_J$ . That is, for all orientations  $\theta''_k$ , the Hamiltonian  $\hat{H}$  in Eq. (18) and  $|\Phi(\theta''_k)\rangle$  describe degenerate (or collapsed) rotational states with the same energy  $E_J$ , a feature well-known for an anisotropic

<sup>5</sup> For any other angle prescription, higher order terms in  $\hat{J}_k$  coupled to intrinsic (such as shear) operators would appear in Eq. (18) [arXiv:1609.04267, arXiv:1610.08337, arXiv:1708.03326]. Therefore, the collective rigid-flow velocity-field prescription in Eq. (19) accounts in an optimum way for the interaction between the rotation and intrinsic motions, which is manifested in the appearance of the rigid-flow kinematic moment of inertia  $\hat{\mathcal{J}}_k$  in

Eqs. (18) and (20). The absence of coupling terms between the rotation and intrinsic motions in Eq. (18) obtained using the unitary transformation in Eq. (17) and the rigid-flow velocity-field prescription in Eq. (19) is also obtained in [99] in a canonical transformation of the kinetic energy using a projection operator for the rotation Lie algebra  $so(3)$ , which decomposes each single-particle momentum into a rigid-flow collective momentum component and its complementary orthogonal intrinsic momentum.



distribution of a system of particles [28 page 475]. Hence, we may conclude that  $\hat{H}$  is an intrinsic Hamiltonian and  $|\Phi(\theta_k'')\rangle$  is an intrinsic deformed wavefunction that is a superposition of angular-momentum eigenstates for a system with the kinematic moments of inertia  $M_{\mathcal{J}_k}$ . Indeed, we observe in Eq. (18) that the collective rotational kinetic energy is subtracted from the nuclear Hamiltonian  $\hat{H}'_o$ , leaving us with the intrinsic Hamiltonian  $\hat{H}$ <sup>6</sup>. One can easily show that:

$$[\theta_k'', \hat{H}] = \frac{-i\hbar}{\hat{\mathcal{J}}_k} \left( \frac{\hat{Q}_{kl}}{\hat{\mathcal{J}}_l} \hat{J}_l + \frac{\hat{Q}_{kk'}}{\hat{\mathcal{J}}_{k'}} \hat{J}_{k'} \right) \approx 0, \quad (21)$$

$$(k \neq l \neq k' = 1, 2, 3)$$

since  $\hat{Q}_{lk}$  for  $k \neq l$  is very small compared to  $\hat{\mathcal{J}}_l$  (as shown below). The result in Eq. (21) is a further indication that  $\hat{H}$  in Eq. (18) is optimally or ideally intrinsic. The Hamiltonian  $\hat{H}$  is also time-reversal and rotationally invariant since the rotation operator  $e^{i\vec{\theta}'' \cdot \hat{\mathbf{J}}/\hbar}$  in Eq. (17) is rotationally invariant (refer to Appendix A).

The inverse of the rigid-flow moment of inertia  $\hat{\mathcal{J}}_l$  is a many-body operator. To render Eq. (18) solvable, we replace  $\hat{\mathcal{J}}_l$  in Eq. (18) by its expectation value (rendering Eq. (18) non-linear):

$$\mathcal{J}_l \equiv \langle \Phi | \hat{\mathcal{J}}_l | \Phi \rangle \quad (22)$$

This is a reasonably good approximation since  $\mathcal{J}_l$  is a relatively large number and varies little and gradually with  $J$ . Eq. (18) then becomes:

$$\begin{aligned} \hat{H} |\Phi(\bar{\theta}'')\rangle &= \left( \hat{H}'_o - \sum_{l \neq k=1}^3 \frac{\hat{J}_k^2}{2M_{\mathcal{J}_k}} - \sum_{l \neq k=1}^3 \frac{\hat{Q}_{lk}}{2M_{\mathcal{J}_l \mathcal{J}_k}} \cdot \hat{J}_l \cdot \hat{J}_k \right) |\Phi(\bar{\theta}'')\rangle \\ &= E_J |\Phi(\bar{\theta}'')\rangle \end{aligned} \quad (23)$$

We now apply to Eq. (23) HF variational and second quantization methods to obtain:

$$\begin{aligned} \hat{H} |\Phi\rangle &= \left[ \hat{H}_{crHF} + \hat{V}_{res} - \sum_{k=1}^3 \frac{(\hat{J}_k^2)_{res}}{2M_{\mathcal{J}_k}} \right] |\Phi\rangle \\ &= E_J |\Phi\rangle \end{aligned} \quad (24)$$

where  $\hat{H}_{crHF}$  is the HF mean-field independent-particle part of  $\hat{H}$  and satisfies the Schrodinger equation:

$$\begin{aligned} \hat{H}_{crHF} |\Phi_{crHF}\rangle &\equiv \left( \hat{H}_{oHF} - \vec{\Omega} \cdot \vec{\hat{J}} - \sum_{l \neq k=1}^3 \frac{Q_{lk}}{\mathcal{J}_k} \cdot \Omega_l \cdot \hat{J}_k - \frac{1}{2} \sum_{l \neq k=1}^3 \Omega_k \cdot \Omega_l M \hat{Q}_{lk} \right) |\Phi_{crHF}\rangle \\ &\equiv E_{J_{crHF}} |\Phi_{crHF}\rangle \end{aligned} \quad (25)$$

where  $Q_{lk} \equiv \langle \Phi_{crHF} | \hat{Q}_{lk} | \Phi_{crHF} \rangle \equiv \langle \hat{Q}_{lk} \rangle$ , and  $\langle \rangle$  denotes the expectation value over the HF state  $|\Phi_{crHF}\rangle$ .  $\hat{H}_{oHF}$  in Eq. (25) is the HF mean-field independent-particle part of the nuclear Hamiltonian  $\hat{H}'_o$ .  $\vec{\Omega} \cdot \vec{\hat{J}}$  in Eq. (25) is the single-particle direct HF mean-field part of  $\sum_{k=1}^3 \frac{\hat{J}_k^2}{2M_{\mathcal{J}_k}}$ , and  $\vec{\Omega}$  is the angular-velocity vector with the magnitude  $\Omega$  and

<sup>6</sup> In many studies [63,100-103], the operator  $\sum_{k=1}^3 \hat{J}_k^2 / \mathcal{J}_k'$  with some inertia parameters  $\mathcal{J}_k'$  has been used to remove spurious rotational excitation

energy. The above results then show that for this removal to be optimal,  $\mathcal{J}_k'$  must be replaced by  $M_{\mathcal{J}_k}$ .

orientation  $(\theta, \phi)$ , and is defined by its three Cartesian components:

$$\begin{aligned}\vec{\Omega} &\equiv (\Omega_1, \Omega_2, \Omega_3) \\ &\equiv \Omega (\sin \theta \cos \phi, \sin \theta \sin \phi, \cos \theta) \\ &= \left( \frac{\langle \hat{J}_1 \rangle}{M \mathcal{J}_1}, \frac{\langle \hat{J}_2 \rangle}{M \mathcal{J}_2}, \frac{\langle \hat{J}_3 \rangle}{M \mathcal{J}_3} \right)\end{aligned}$$

(26)

$(\hat{J}_i^2)_{res}$  in Eq. (24) is the residual of the square of the angular-momentum operator given by [arXiv:1810.11836, arXiv:1909.07169]:

$$\begin{aligned}(\hat{J}_i^2)_{res} &\equiv \hat{J}_i^2 - 2 \langle \Phi_{crHF} | \hat{J}_i | \Phi_{crHF} \rangle \cdot \hat{J}_i \\ &= \sum_{\nu, \nu'=1}^{\infty} \left[ (\hat{J}_i^2)_{\nu\nu'} - 2 \sum_{k=1}^A (\hat{J}_i)_{\nu k} \cdot (\hat{J}_i)_{k\nu'} \right] \cdot a_{\nu}^{\dagger} a_{\nu'} \\ &\quad + \sum_{l,k=1}^A (\hat{J}_i)_{lk} \cdot (\hat{J}_i)_{kl} - \langle \hat{J}_i \rangle^2 \\ &\quad + \sum_{\substack{\mu, \mu' \\ \nu, \nu'=1}}^{\infty} (\hat{J}_i)_{\mu\mu'} \cdot (\hat{J}_i)_{\nu\nu'} : a_{\mu}^{\dagger} a_{\nu}^{\dagger} a_{\nu'} a_{\mu'} : \end{aligned} \quad (27)$$

For the residual of nuclear interaction  $\hat{V}_{res}$  in Eq. (24), we may use the separable effective quadrupole-quadrupole (long range) interaction (which is often used in nuclear structure calculations):

$$\begin{aligned}\hat{V}_{res} &= -\frac{\chi}{2} \hat{Q}^{\dagger} \cdot \hat{Q}, \\ \hat{Q}_{\mu} &\equiv \sum_{n=1}^A (r_n^2 \hat{q}_{n\mu} - \langle r_n^2 \hat{q}_{n\mu} \rangle), \\ \hat{q}_{n\mu} &\equiv Y_{2\mu}(\theta_n, \phi_n), \quad \mu = 0, \pm 1, \pm 2\end{aligned} \quad (28)$$

where the parameter  $\chi$  is the interaction strength. In Eq. (24) we do not show the

residual of the three-body operator

$-\sum_{l \neq k=1}^3 \frac{\hat{Q}_{lk}}{2M \mathcal{J}_l \mathcal{J}_k} \cdot \hat{J}_l \cdot \hat{J}_k$  because it is negligibly small, complicated, and is not used in this article.

The terms in  $Q$  in the Hamiltonian

$\hat{H}_{crHF}$  in Eq. (25) are very small, contributing less than 0.1%<sup>7</sup>, and therefore they are neglected, and Eq. (25) becomes:

$$\begin{aligned}\hat{H}_{crHF} | \Phi_{crHF} \rangle &= \left( \hat{H}_{oHF} - \vec{\Omega} \cdot \vec{\hat{J}} \right) | \Phi_{crHF} \rangle \\ &= E_{JcrHF} | \Phi_{crHF} \rangle\end{aligned} \quad (29)$$

MSCRM3 Eq. (29) is identical in form to CCRM3 Eq. (1) except for the microscopically determined angular-velocity vector  $\vec{\Omega}$ . Taking the expectation of Eq. (29), we obtain the intrinsic energy:

$$\begin{aligned}E_{int} \equiv E_{JcrHF} &= \langle \hat{H}_{oHF} - \vec{\Omega} \cdot \vec{\hat{J}} \rangle \\ &= \hbar \sum_{k=1}^3 \alpha_k \Sigma_k\end{aligned} \quad (30)$$

where the normal-mode frequencies  $\alpha_k$  are given in Eq. (6) since Eqs. (29) and (1) are identical in form.

In Eq. (29),  $| \rangle \equiv | \Phi_{crHF} \rangle$  is required to satisfy Eqs. (31) given below instead of Eq. (13) or (14). The value  $J_{cal}$  of the true (rather than the imposed  $J$ ) angular momentum quantum number, calculated

<sup>7</sup> We now determine  $Q_{lk} \equiv \langle \hat{Q}_{lk} \rangle$  in Eq. (25) by inserting  $\hat{H}_{crHF}$  in Eq. (25) into  $\langle [\hat{H}_{crHF}, \hat{J}_k] \rangle = 0$ , which is valid because  $| \rangle$  is an eigenstate of  $\hat{H}_{crHF}$ . We then obtain  $Q_{lk} = -(\mathcal{J}_l - \mathcal{J}_k) \Omega_l \Omega_k / (\omega_l^2 - \omega_k^2)$

( $k \neq l$ ) when we ignore the terms in  $Q$  in  $\hat{H}_{crHF}$  in Eq. (25), and determine that  $Q_{ij} / \hat{\mathcal{J}}_i < 0.1\%$ . With the terms  $Q$  in  $\hat{H}_{crHF}$  included, the expressions for  $Q_{lk}$  are complicated but we expect them to yield a slightly larger value but still less than 0.2%.

from Eqs. (10) and (30), is given by:

$$J_{cal} = \begin{cases} 0.5 \left( -1 + \sqrt{1 + 4 \langle \hat{J} \rangle^2} \right) & \text{for triaxial rotation} \\ \sqrt{\langle \hat{J} \rangle^2} & \text{for uniform rotation} \end{cases} \quad (31)$$

$$\langle \hat{J} \rangle^2 \equiv \langle \hat{J}_1 \rangle^2 + \langle \hat{J}_2 \rangle^2 + \langle \hat{J}_3 \rangle^2$$

It is clear from Eqs. (13), (14), and (31) that  $J_{cal}$  and  $J$  do not generally have the same value.

The orientation  $(\theta, \phi)$  and the magnitude  $\Omega$  of the angular-velocity vector  $\vec{\Omega}$  are readily determined from the rigid-flow angular-velocity prescription in Eq. (26), and are given by:

$$\tan \phi = \frac{\langle \hat{J}_2 \rangle_{\mathcal{J}_1}}{\langle \hat{J}_1 \rangle_{\mathcal{J}_2}}, \quad (32)$$

$$\tan \theta = \frac{\langle \hat{J}_1 \rangle_{\mathcal{J}_3}}{\langle \hat{J}_3 \rangle_{\mathcal{J}_1}} \sqrt{1 + \tan^2 \phi}$$

$$\begin{aligned} \Omega^2 &= \Omega_1^2 + \Omega_2^2 + \Omega_3^2 \\ &= \frac{\langle \hat{J}_1 \rangle^2}{M^2 \mathcal{J}_1^2} + \frac{\langle \hat{J}_2 \rangle^2}{M^2 \mathcal{J}_2^2} + \frac{\langle \hat{J}_3 \rangle^2}{M^2 \mathcal{J}_3^2} \\ &= (T_1 + T_2 + T_3)/3 \end{aligned} \quad (33)$$

where:

$$\begin{aligned} T_1 &\equiv \frac{\langle \hat{J}^2 \rangle}{M^2 \mathcal{J}_3^2} + \left( \frac{1}{M^2 \mathcal{J}_1^2} - \frac{1}{M^2 \mathcal{J}_3^2} \right) \langle \hat{J}_1 \rangle^2 \\ &\quad + \left( \frac{1}{M^2 \mathcal{J}_2^2} - \frac{1}{M^2 \mathcal{J}_3^2} \right) \langle \hat{J}_2 \rangle^2 \end{aligned}$$

$$\begin{aligned} T_2 &\equiv \frac{\langle \hat{J}^2 \rangle}{M^2 \mathcal{J}_2^2} \\ &\quad + \left( \frac{1}{M^2 \mathcal{J}_1^2} - \frac{1}{M^2 \mathcal{J}_2^2} \right) \langle \hat{J}_1 \rangle^2 \\ &\quad + \left( \frac{1}{M^2 \mathcal{J}_3^2} - \frac{1}{M^2 \mathcal{J}_2^2} \right) \langle \hat{J}_3 \rangle^2 \\ T_3 &\equiv \frac{\langle \hat{J}^2 \rangle}{M^2 \mathcal{J}_1^2} \\ &\quad + \left( \frac{1}{M^2 \mathcal{J}_2^2} - \frac{1}{M^2 \mathcal{J}_1^2} \right) \langle \hat{J}_2 \rangle^2 \\ &\quad + \left( \frac{1}{M^2 \mathcal{J}_3^2} - \frac{1}{M^2 \mathcal{J}_1^2} \right) \langle \hat{J}_3 \rangle^2 \end{aligned}$$

where in  $T_1$ ,  $T_2$ , and  $T_3$  in Eq. (33),

$\langle \hat{J}^2 \rangle = \langle \hat{J}_1 \rangle^2 + \langle \hat{J}_2 \rangle^2 + \langle \hat{J}_3 \rangle^2$ . In Eq. (33), we

set  $\langle \hat{J}^2 \rangle$  equal to either  $\hbar^2 J^2$  for principal-

axis rotation or to  $\hbar^2 J(J+1)$  for triaxial rotation, with  $J$  taking on the desired quantum value to be imposed on the wavefunction, as in Eqs. (13) and (14). Eq. (33) is examined further in Section 4 where we discuss rotational instability and its stabilization.

The independent-particle cranking model Schrodinger Eq. (29), the angular velocity Eqs. (32) and (33), the wavefunction angular-momentum constraint (i.e., the true angular-momentum quantum number  $J_{cal}$ ) in Eq. (31) constitute a quantum, microscopic, self-consistent, time-reversal and  $D_2$  invariant, parameter-free cranking model for triaxial rotation (MSCRM3). MSCRM3 may be considered a quantum, microscopic parameter-free analogue of CCRM3.

The above derivation of MSCRM3 reveals the approximations and assumptions implied by CCRM3, and its limitations.

Specifically, in MSCRM3: **(i)** the rigid-flow angular-velocity prescription in Eqs. (19), (20), and (26) ensures that the Hamiltonian  $\hat{H}$  in Eq. (18) is optimally intrinsic as defined in Eq. (21); for any other prescription,  $\hat{H}$  in Eq. (18) and hence  $\hat{H}_{crHF}$  in Eq. (29) will contain higher order terms in  $\hat{J}_k$  coupled perhaps strongly to intrinsic operators, complicating the solution method of its Schrodinger equation and possibly requiring using additional approximations and assumptions, thereby complicating a comparison of MSCRM with CCRM3; clearly, the CCRM3 Hamiltonian  $\hat{H}_{cr}$  in Eq. (1) is not optimally intrinsic since  $\vec{\Omega}$  in Eq. (1) is an arbitrary parameter; however, for uniaxial rotation, CCRM1 yields approximately the rigid-flow dynamic moment of inertia when the density-potential self-consistency condition is used [5,11,13,22,27], **(ii)** the prescription for  $\Omega_k$  in Eq. (26) allows  $\Omega_k$  and  $\langle \hat{J}_k \rangle$  to be determined self-consistently and completely<sup>8</sup> via Eqs. (32) and (33), **(iii)** CCRM3 Eq. (12) is inconsistent with MSCRM3 Eq. (32): Eq. (32) shows that, in MSCRM3,  $\vec{\Omega}$  and  $\langle \vec{\hat{J}} \rangle$  are not parallel vectors, meaning that

---

<sup>8</sup> Note that, if we use Eq. (26) to determine  $\Omega_k$  instead of the constraint in Eq. (33), then the rotational states would decay to the ground state because of the strong coupling between the rotational and intrinsic motions and the resulting flow of energy between them and the positive feedback between  $\Omega_k$  and  $\langle \hat{J}_k \rangle$ . Indeed, when we keep the oscillator frequencies constant at their values at some  $J_{cal}=J_{stop}$  and in the subsequent iteration steps, the decay stops when  $J_{cal}$  reaches  $J_{stop}$ . We have shown in previous

the rotation is generally not uniform but wobbly (i.e., the orientation  $(\theta, \phi)$  of  $\vec{\Omega}$  defined in Eq. (32) is not the same as the orientation  $(\theta_J, \phi_J)$  of  $\langle \vec{\hat{J}} \rangle$  defined by

$$\tan \phi_J = \frac{\langle \hat{J}_2 \rangle}{\langle \hat{J}_1 \rangle} \quad \text{and} \quad \tan \theta_J = \frac{\langle \hat{J}_1 \rangle}{\langle \hat{J}_3 \rangle} \sqrt{1 + \tan^2 \phi_J}$$

)) unless  $\langle \hat{J}_2 \rangle = \langle \hat{J}_3 \rangle = 0$ ,  $\mathcal{J}_1 = \mathcal{J}_2$  and  $\langle \hat{J}_3 \rangle = 0$ , or  $\langle \hat{J}_1 \rangle = \langle \hat{J}_3 \rangle = 0$ ,  $\mathcal{J}_1 = \mathcal{J}_3$ ). On the other hand, Eq. (12) shows that in CCRM3  $\vec{\Omega}$  and  $\langle \vec{\hat{J}} \rangle$  are always parallel

vectors; **(iv)** MSCRM3 Schrodinger equation is self-consistent, parameter-free, time-reversal and  $D_2$  and hence signature invariant, (because  $\Omega_k$  in Eq. (26) changes sign under time reversal and rotation through  $\pi$  about each principal axis, and hence MSCRM3 wavefunction is a superposition of either even or odd  $J_{cal}$  angular momentum eigenstates, whereas a CCRM3 wavefunction is a superposition of even and odd  $J$  eigenstates. This MSCRM3 feature resolves the difficulty of relating the

predicted and experimentally observed rotational bands pointed out in [47]; and **(v)** the above MSCRM3 derivation indicates

studies [arXiv:1609.04267, arXiv:1610.08337, arXiv:1708.03326] that a complete separation between collective rotation and other nuclear degrees of freedom is not possible except under some extreme conditions such as very low angular velocities and/or large deformations. Therefore, MSCRM3 does not describe a stable free or self-sustaining rotation. Indeed, one may wonder if stable free self-sustaining rotation at a constant angular momentum is possible in a self-consistent system of particles.

that CCRM3 neglects the correction terms

$$-\sum_{l \neq k=1}^3 \frac{\hat{Q}_{lk}}{2M \mathcal{G}_l \mathcal{G}_k} \cdot \hat{J}_l \cdot \hat{J}_k \text{ (which is in fact negligibly small) and } -\sum_{k=1}^3 \frac{(\hat{J}_k^2)_{res}}{2M \mathcal{G}_k} \text{ (which$$

#### 4. MSCRM3 and CCRM3 predictions and their differences

The coupled algebraic CCRM3 Eqs. (6), (9), (10), (11), (12), (13), and (14) and MSCRM3 Eqs. (6), (10), (11), (22), (29), (30), (31), (32), and (33) are similar in form. Therefore, for a deformed self-consistent harmonic-oscillator potential<sup>9</sup>, these two sets of equations are solved iteratively in a similar manner over the entire allowed range of  $J$  in nuclei <sup>20</sup>Ne, <sup>24</sup>Mg, and <sup>28</sup>Si.

CCRM3 Eq. (12) shows that as  $\langle \hat{J}_k \rangle$  varies in the iteration process, so do  $\phi'$  and  $\theta'$ . We indicate by  $\phi'_o$  and  $\theta'_o$  the values of  $\phi'$  and  $\theta'$  at the start of the iterative-solution procedure. For  $J=2$  in CCRM3, we calculate  $\langle \hat{J}_k \rangle$  from Eq. (10),  $\langle x_k^2 \rangle$  from Eq. (10), and  $\omega_k^2$  from Eq. (11) in the first iteration step using the values of  $\omega_k^2$  and  $\langle x_k^2 \rangle$  at  $J=0$ , the desired values of  $\phi'_o$ , and  $\theta'_o$ , and a guessed value of  $\Omega$ . The calculated values of  $\langle \hat{J}_k \rangle$ ,  $\langle x_k^2 \rangle$ , and  $\omega_k^2$  are then used in the next iteration step to calculate the next set of values of the variables, and so on until converged values are obtained. Then, we compute the values of  $E_J$  and  $\Delta E_J$  in Eqs. (15) and the quadrupole moment

includes a part of the HF one-body direct and exchange terms and other residual parts of the square of the angular momentum operator), which is estimated in Section 4 to have significant impact on the excitation energies.

$Q \equiv Z \cdot e \cdot (2\langle z^2 \rangle - \langle x^2 \rangle - \langle y^2 \rangle) / A$  for each value of  $J$ . These converged values are used in the iteration procedure for  $J=2$  and higher  $J$  values.

The above iterative procedure is also used for MSCRM3 (note that, since we are choosing the values of  $\phi_o$  and  $\theta_o$  in the first iteration step, we do not need to know the values of  $\langle \hat{J}_k \rangle$  to evaluate  $\phi_o$  and  $\theta_o$  in Eq. (32) in the first iteration step). For a desired value of  $J_d$  of  $J$ , we determine  $\Omega^2$  from Eq. (33),  $\langle \hat{J}_k \rangle$  from Eq. (10), and  $J_{cal}$  from Eq. (31). If  $J_{cal} \neq J_d$ , we choose a smaller or larger value of  $J$  until  $J_{cal}=J_d$ ,

The CCRM3 and MSCRM3 equations involve expectations of operators with respect to the cranked wavefunction. Therefore, these equations are non-linear and hence may have oscillatory solutions. To avoid oscillatory solutions and obtain steady converged rotations, the input and output values of the variables in each iteration step are linearly mixed and used as input in the next iteration step. Although the linear-mixing method works well here, a more accurate approach to obtaining converged solution is to use other more convergent iterative methods such as Broyden's method [104,105,106].

We use the following ground-state nucleon deformed-harmonic-oscillator configurations. For the <sup>20</sup>Ne ground state, the deformed harmonic-oscillator single-

<sup>9</sup> We have also added the spin-orbit  $\vec{l} \cdot \vec{s}$  term in this formalism. An estimate of the impact of the spin-orbit from this analysis is presented below.

particle model predicts an axially-symmetric prolate shape with a nucleon configuration having the total oscillator-phonon quantum numbers  $\Sigma_k = (14,14,22)$  [7,14,21,107,108,109]. For  $^{24}\text{Mg}$  ground state, it predicts an axially-symmetric prolate shape with  $\Sigma_k = (20,20,24)$ , and a triaxial shape with  $\Sigma_k = (16,20,28)$  [14,21,108,109,110]. For  $^{28}\text{Si}$  ground state, it predicts a prolate axially-symmetric shape with  $\Sigma_k = (22,22,34)$ , an oblate axially-symmetric shape with  $\Sigma_k = (30,30,18)$ , and two ellipsoidal shapes with  $\Sigma_k = (26,22,30)$  and  $\Sigma_k = (30,26,22)$  [14,18,109,110].

Since the governing CCRM3 and MSCRM3 equations are similar in form, their predictions are similar. But there are also some significant differences. We now present in items A to L below the major predictions of CCRM3 and MSCRM3 and the major differences between these predictions for nuclei  $^{20}\text{Ne}$ ,  $^{24}\text{Mg}$ , and  $^{28}\text{Si}$ . We also compare these predictions with those of CCRM3 reported in [45-48,51,54].

- A.** The CCRM3 and MSCRM3 rotational states are inherently unstable because of the intrinsic-system destabilizing positive-feedback mechanism between  $\Omega_k$  and  $\langle \hat{J}_k \rangle$ . This feedback is generated by the first of Eqs. (10) and the self-consistency-condition in Eq. (11), which create strong coupling between the rotation and intrinsic motions. Fig. 1 shows that the CCRM3 (or MSCRM3) predicted excited-state

energy  $E_J$  in Eq. (15) typically increases and the intrinsic energy  $E_{\text{int}}$  in Eq. (9) decreases with  $J^{10}$ . This result implies that the increase in the rotational energy is supplied by a corresponding decrease in the intrinsic energy through changes in the intrinsic kinetic and deformation energies. Since, in Fig. 1,  $\frac{\partial E_{\text{int}}}{\partial \Omega_k} < 0$ , and

because  $\Omega_k$  increases with  $J$ , we conclude, from Eq. (10), that

$$\langle \hat{J}_k \rangle = -\frac{\partial E_{\text{int}}}{\partial \Omega_k} > 0, \text{ and hence } \langle \hat{J}_k \rangle$$

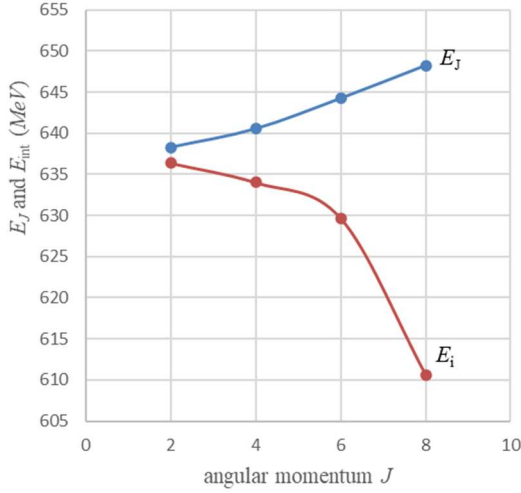
decreases when  $\Omega_k$  decreases.

Therefore, any decrease in  $\langle \hat{J}_k \rangle$  causes  $\Omega_k$  to decrease, which in turn causes  $\langle \hat{J}_k \rangle$  to decrease further thereby reducing  $\langle \hat{J}_k \rangle$  to zero unless this free fall is prevented by some constraint<sup>11</sup>.

<sup>10</sup> The excited-state energies  $E_J$  and  $E_{\text{int}}$  shown in Figure 1 are the energies obtained from Eqs. (9) and (15) by filling the deformed harmonic oscillator subshells with  $A$  nucleons. For convenience, the negative minimum of the oscillator potential is shifted upward to the zero value because we are interested in excitation energies (from which the ground-state energy is subtracted) and not excited-state energies.

<sup>11</sup> This result, which can be demonstrated using MSCRM3 (refer to footnote 9), implies that a stable free self-sustaining cranked rotational state is not possible. This results also implies that this instability occurs for any self-consistent mean-field potential and not just for the oscillator potential.

Fig. 1: CCRM3 calculated excited-state energy  $E_J$  (Eq (15)) and intrinsic energy  $E_{\text{int}}$  (Eq (9)) versus  $J$  for  $\phi_o = 40^\circ$  in  $^{20}\text{Ne}$



- B.** For a given non-zero  $J$  imposed externally on  $\langle \hat{J}^2 \rangle$  in Eqs. (13) and (14) or Eq. (31), a CCRM3 or MSCRM3 rotational state does not totally collapse rotationally (i.e., all three components  $\langle \hat{J}_k \rangle$  decrease to zero). For this reason and as seen in Fig. 2,  $\langle \hat{J}_3 \rangle$  normally reduces to zero and hence  $\theta$  increases to  $90^\circ$  after a few iteration steps at  $J=2$  or at a higher  $J$ , resulting in a planar uniform rotation in the  $x$ - $y$  plane in CCRM3 and planar wobbly rotation in the  $x$ - $y$  plane in MSCRM3<sup>12</sup>. Then, any small decrease in, for example,  $\langle \hat{J}_1 \rangle$

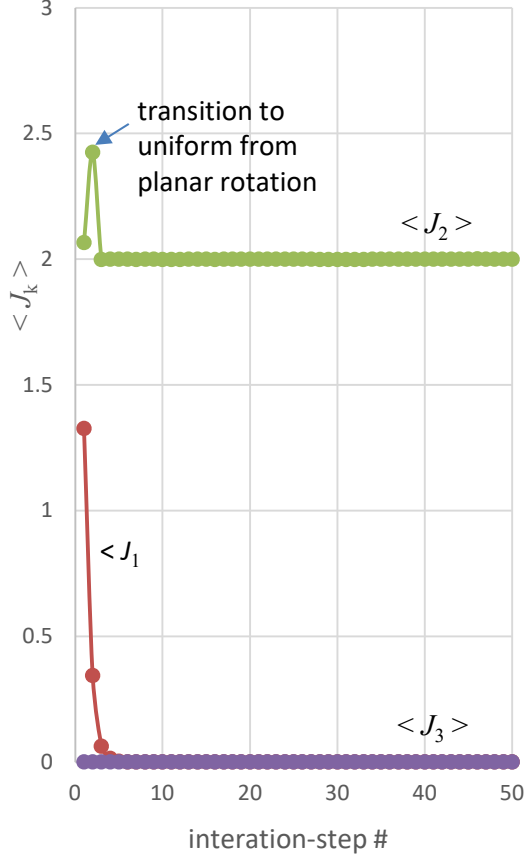
results in a monotonic decrease in  $\langle \hat{J}_1 \rangle$  and an increase in  $\langle \hat{J}_2 \rangle$  and hence  $\phi$ , resulting in a uniform rotation about the principal  $y$  axis. Similarly, for any small decrease in  $\langle \hat{J}_2 \rangle$  in the iteration process, the positive feedback causes  $\langle \hat{J}_2 \rangle$  and hence  $\phi$  to monotonically decrease to zero and  $\langle \hat{J}_1 \rangle$  to increase to  $J$ , resulting in a uniform rotation about the principal  $x$  axis (as demonstrated in Fig. 2). An exception to these two cases is when the planar rotation is about the  $\phi = 45^\circ$  line in the  $x$ - $y$  plane in which case the planar uniform rotation is stable in CCRM3 but not in MSCRM3, as in the  $^{20}\text{Ne}$  case discussed below<sup>13</sup>. In Fig. 2 we do not show the results predicted for  $^{28}\text{Si}$  beyond 50 iteration steps because neither MSCRM3 nor CCRM3 predict any physically meaningful rotations beyond 100 iteration steps.

<sup>12</sup> Refer to the discussion in item (iii) in the last paragraph in Section 3 for the general rotational types predicted by CCRM3 and MSCRM3.

<sup>13</sup>In the CCRM3 case in Fig. 2 for  $^{28}\text{Si}$ , the  $\Omega^2$  had to be slightly increased in each iteration step to maintain the angular momentum at the desired value  $J=2$ . Eventually, after some iterations, CCRM3 equations predicted a large value of  $J$  independent of the value of  $\Omega^2$ . This result indicates an anomaly in the derivatives of the cranked-harmonic-oscillator normal-mode frequencies. It may also indicate the need to use a more accurate iteration solution method such as Broyden's method [104,105,106]. To avoid

oscillatory solutions to the non-linear CCRM3 and MSCRM3 equations, the computer program currently uses a linear mixing of the input and output variables in each iteration step as input in the next iteration step. In some cases, if the linear mixing is not used, the angular velocity would be oscillatory at a constant value of the angular momentum or else the angular momentum would be oscillatory at a constant angular velocity. Refer to footnote 16 and item I for  $^{24}\text{Mg}$  case with  $\phi = 89$  and  $\theta_o = 54.7^\circ$ , and Section J for more detail.

**Fig. 2: CCRM3 predicted  $\varphi$  and  $\langle J_k \rangle$  versus iteration-step # for  $\varphi_0 = 20^\circ$  and  $\theta_0 = 90^\circ$  at  $J=2$  in triaxial  $^{28}\text{Si}$**



- C.** From the results in items A and B above, we conclude that CCRM3 predicts only uniform rotation (about the  $45^\circ$  line in the  $x$ - $y$  plane or about the  $x$  or  $y$  axis with  $\theta=90^\circ$ ), and it does not predict any triaxial rotations where at least two of the three  $\langle \hat{J}_k \rangle$  are non-zero, except for a planar rotation about the  $45^\circ$  line in the  $x$ - $y$  plane. This may or may not be the case in MSCRM3 (as the  $^{24}\text{Mg}$  case discussed below shows).
- D.** The MSCRM3 self-consistency between  $\Omega_k$  and  $\langle \hat{J}_k \rangle$  in Eqs. (26) and (33) may generate fluctuations in these and other

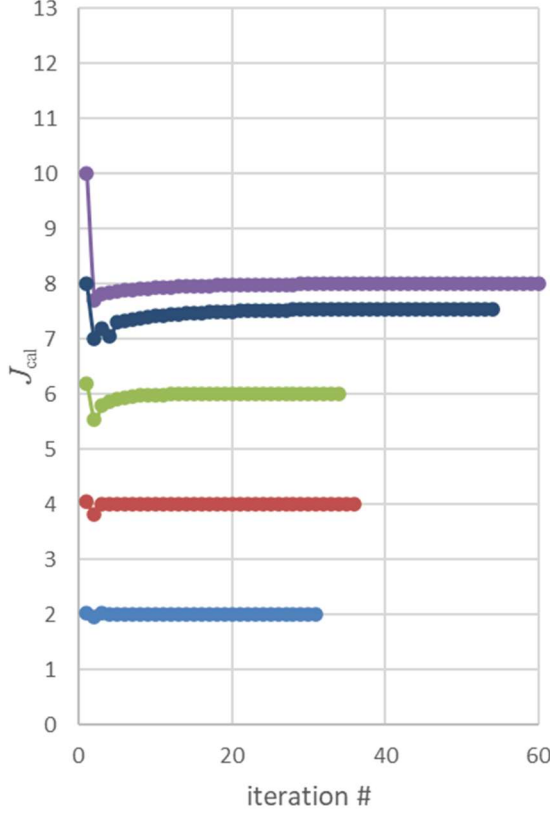
variables, which may cause the MSCRM3 rotational states to be either more (as is the case in  $^{20}\text{Ne}$  discussed below) or less unstable than the CCRM3 states.

- E.** As seen in Fig. 3, the self-consistency between  $\Omega_k$  and  $\langle \hat{J}_k \rangle$  in MSCRM3 also allows the intrinsic system to rotationally relax after the imposed  $J$  in the first iteration step is removed and replaced by Eq. (33). This rotational relaxation yields a value of  $J_{\text{cal}}$  in Eq. (31) that is smaller or larger than  $J$ . For example, for  $J=10$ ,  $J_{\text{cal}}$  decreases from 10 to 8 after the imposed  $J=10$  is removed in the second iteration step and replaced by Eq. (33).

In contrast, CCRM3 forces the intrinsic system to accept a value  $J$  of the angular momentum that may be inconsistent with the nucleonic motion.



**Fig. 3: MSCRM3 calculated  $J_{\text{cal}}$  versus iteration # for  $\phi_o=40^\circ$  showing rotational relaxation from higher initial  $J$  in  $^{20}\text{Ne}$**



- F.** The arbitrary values of  $\phi_o$  and  $\theta_o$  at the start of the iteration process determine the nature of the subsequent rotation. For  $\phi_o=45^\circ$  and  $\theta_o=90^\circ$ , the planar rotation in the  $x$ - $y$  plane is stable in CCRM3, but it is unstable in MSCRM3 because of the fluctuations in  $\langle \hat{J}_1 \rangle$  and  $\langle \hat{J}_2 \rangle$  allowed by Eqs. (26) and (33).
- G.** For **prolate**  $^{20}\text{Ne}$  (axially-symmetric about  $z$  axis),  $\phi_o=45^\circ$ , and  $\theta_o>0^\circ$  (which increases to  $90^\circ$  in the first few iteration steps), **MSCRM3** predicts a

planar rotation in the  $x$ - $y$  plane at  $J_{\text{cal}} \leq 6$  (relaxed from  $J = 6.6$ ). At  $J_{\text{cal}} = 7.76$  (relaxed from  $J = 8$ ),  $^{20}\text{Ne}$  becomes triaxial (due to interaction between centrifugal stretching and incompressibility condition), and the fluctuations in  $\langle \hat{J}_1 \rangle$  and  $\langle \hat{J}_2 \rangle$  are amplified in  $\langle \hat{J}_2 \rangle$  reducing it to zero.

This causes a transition to uniform rotation about the  $x$  axis (i.e., quenching of the wobbly rotation) and the switching from the constraint  $\langle \hat{J}^2 \rangle = \hbar^2 J(J+1)$  to  $\langle \hat{J}^2 \rangle = \hbar^2 J^2$ . At  $J_{\text{cal}} = 8$  ( $= (\Sigma_3 - \Sigma_1) = (22 - 14)$ ) (relaxed from  $J = 10$ ),  $^{20}\text{Ne}$  becomes axially symmetric about the  $x$  axis and the rotational band terminates. The quenching of the wobbly rotation reduces the energy-level spacing between  $J_{\text{cal}}=6$  and 8 and improves the agreement with the measured excitation energy as seen in Fig. 4<sup>14</sup>. The remaining discrepancy between the measured and MSCRM3-predicted excitation energies in Fig. 4 is partly due to the neglect of the spin-orbit interaction, which we have shown to increase the predicted energy by 10%. The remaining discrepancy is due to the neglect of the residuals of  $\hat{J}_k^2$  and  $V$  in Eq. (24), which is estimated, in MSCRM1 for uniaxial rotation [arXiv:1810.11836] using Tamm-Dancoff approximation and cranked 1-particle 1-hole basis states, to be 1 to 2 MeV (as seen in Fig. 5) increasing the predicted excitation energy close to the measured excitation energy.

In contrast, in **CCRM3** the uniform

<sup>14</sup> This reduction in energy-level spacing has been known [5,7] but has not been attributed to any specific phenomenon. MSCRM3 attributes this

phenomenon to the transition from a wobbly planar to a uniform rotation (in other words, to the quenching of wobbling) at  $J=8$ .

planar rotation of  $^{20}\text{Ne}$  about the  $\phi_0 = 45^\circ$  line in the  $x$ - $y$  plane persists at all  $J$  values with increasing excitation energy and no rotational-band termination as seen in Fig. 4.

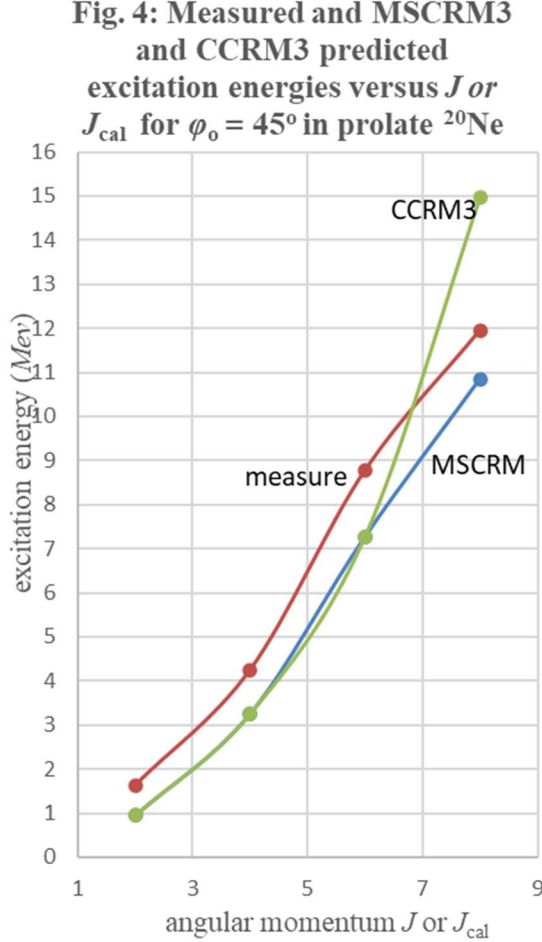
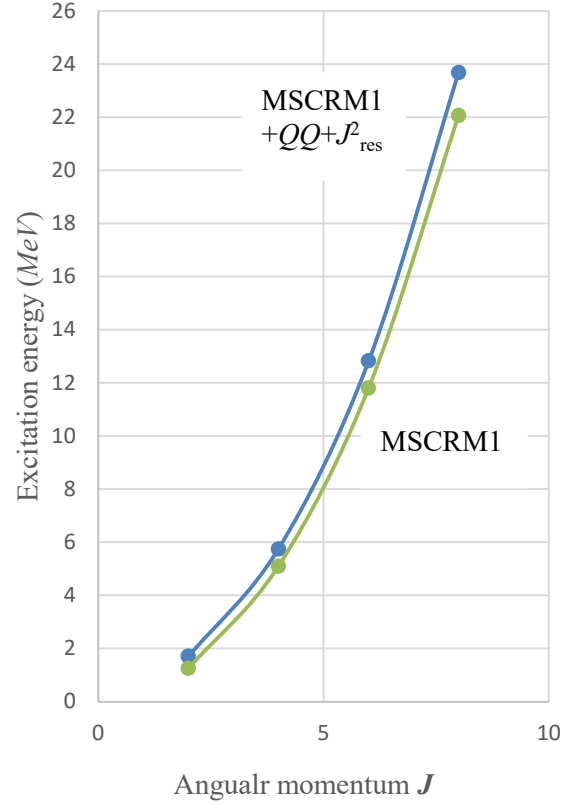
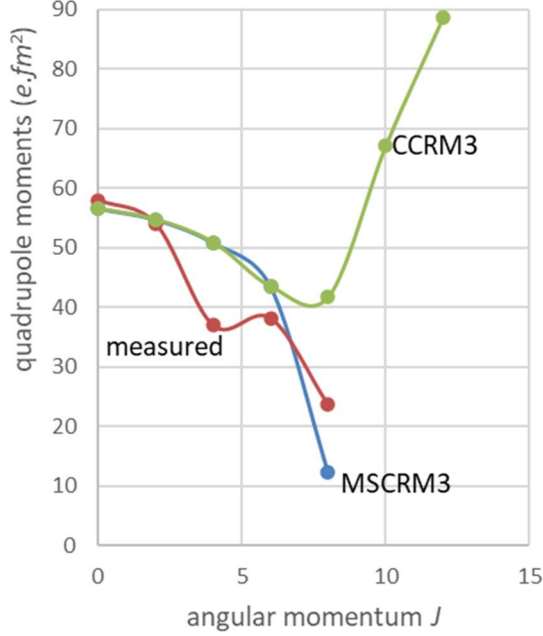


**Fig. 5: MSCRM1 predicted excitation energy versus  $J$  in  $^{20}\text{Ne}$  for uniform rotation without and with  $Q, Q$  and  $J^2_{\text{res}}$  residuals using cranked 1-particle and 1-hole states**



For  $^{20}\text{Ne}$  and  $\phi_0 = 45^\circ$ , CCRM3 and MSCRM3 predict similar **quadrupole moments**  $Q$  up to  $J=6$ , as seen in Fig. 6 (where  $Q \equiv \frac{Z \cdot e}{A} \cdot (2\langle z^2 \rangle - \langle x^2 \rangle - \langle y^2 \rangle)$ , measured values are from [5,109,110]). Above  $J=6$ , MSCRM3 predicts that  $Q$  decreases sharply because of the transition from wobbly to uniform rotation at  $J=8$  ( $=(\Sigma_3 - \Sigma_1) = (22 - 14)$ ) and to an axially symmetric nucleus, whereas CCRM3 predicts that  $Q$  increases without limit since the rotational band does not terminate.

**Fig. 6: MSCRM3 & CCRM3  
predicted & measured  
quadrupole moments versus  $J$   
for  $\phi_o = 45^\circ$  in  $^{20}\text{Ne}$**



For  $\phi_o \neq 45^\circ$  in  $^{20}\text{Ne}$ , CCRM3 and MSCRM3 predict respectively uniform and wobbly planar rotations at low  $J$  or  $J_{\text{cal}}$  values. At higher  $J$  or  $J_{\text{cal}}$  values,  $^{20}\text{Ne}$  becomes triaxial and the rotation becomes uniform about the  $x$  axis for  $\phi_o < 45^\circ$ , and about the  $y$  axis for  $\phi_o > 45^\circ$ . At  $J$  or  $J_{\text{cal}}=8$  ( $=(\Sigma_3 - \Sigma_1) = (22 - 14)$ ),  $^{20}\text{Ne}$  becomes axially symmetric about the  $x$  or  $y$  axis and the rotational band terminates.

**H. For prolate  $^{24}\text{Mg}$  and  $^{28}\text{Si}$ , and  $\phi_o = 45^\circ$ , MSCRM3 predicts a wobbly (i.e., non-uniform) planar rotation in the  $x$ - $y$  plane at respectively  $J_{\text{cal}} < 4$  and 8. At respectively  $J_{\text{cal}}=4$  and 10, the rotation transitions to a uniform rotation about the  $x$  or  $y$  axis and the nuclei become triaxial. At respectively  $J_{\text{cal}}=4$  ( $=\Sigma_3 - \Sigma_2$**

$=24-20$ ) and 12 ( $=\Sigma_3 - \Sigma_2=34-22$ ) the nuclei become axially symmetric about the  $x$  or  $y$  axis and the rotational band terminates. The  $J=12$  excitation energy level in  $^{24}\text{Mg}$  is also predicted in an  $sd$ -shell model calculation [111] and observed in an experiment [112].

In contrast, **for prolate  $^{24}\text{Mg}$  and  $^{28}\text{Si}$ , and  $\phi_o = 45^\circ$ , CCRM3 predicts a planar uniform rotation about the  $45^\circ$  line in the  $x$ - $y$  plane of an axially symmetric (about  $z$  axis) nucleus at all  $J$  values with no band termination.**

**For prolate  $^{24}\text{Mg}$  and  $^{28}\text{Si}$ , and  $\phi_o \neq 45^\circ$ , MSCRM3 and CCRM3 predict that, at respectively  $J < 4$  and 8, the planar rotation in the  $x$ - $y$  plane transitions to a uniform rotation about the  $x$  axis for  $\phi_o < 45^\circ$  and about the  $y$  axis for  $\phi_o > 45^\circ$ .**

At respectively  $J_{\text{cal}}=4$  and 8, the nuclei become axially symmetric about the  $x$  or  $y$  axis and the rotational band terminates.

The above predictions for  $^{24}\text{Mg}$  and  $^{28}\text{Si}$  are similar to those for  $^{20}\text{Ne}$  described in the item H above.

**I. For triaxial  $^{24}\text{Mg}$ ,  $\phi_o = 90^\circ$ , and  $\theta_o = 90^\circ$ , MSCRM3 predicts  $\langle \hat{J}_1 \rangle = \langle \hat{J}_3 \rangle = 0$ , and a steady uniform rotation of a triaxial nucleus about the  $y$  axis at all values of  $J_{\text{cal}}$ . The rotational band does not terminate because the condition  $\phi_o = 90^\circ$ ,  $\theta_o = 90^\circ$  does not allow a transition to a triaxial rotation and the resulting change in the nuclear shape to an axial or a spherical shape (as it happens in the case  $\phi_o = 89^\circ$ ,  $\theta_o = 90^\circ$  describe below).**

**For triaxial  $^{24}\text{Mg}$ ,  $\phi_o = 90^\circ$ , and  $\theta_o = 90^\circ$ ,**

**CCRM3** predicts a similar rotation to that predicted above by **MSCRM3**.

**For triaxial  $^{24}\text{Mg}$ ,  $\phi_o=90^\circ$ , and**

**$0^\circ < \theta_o < 90^\circ$ , **MSCRM3** predicts  $\langle \hat{J}_1 \rangle = 0$**

at all  $J_{\text{cal}}$  values, and a steady planar rotation in the  $y$ - $z$  plane at  $J_{\text{cal}}=2$  and 4, and a uniform steady rotation about the  $y$  axis (i.e.,  $\langle \hat{J}_1 \rangle = \langle \hat{J}_3 \rangle = 0$ , and  $\langle \hat{J}_2 \rangle \neq 0$ )

at  $J=6$ . At  $J=8$ , the nucleus becomes axially symmetric about the  $y$  axis and the rotational band terminates at  $J_{\text{cal}}=8$  ( $=\Sigma_3 - \Sigma_2 = 28-20$ ) and not, as may be expected, at  $J_{\text{cal}}=12$  ( $=\Sigma_3 - \Sigma_1 = 28-16=12$ ), in contrast to the case for  $\phi_o=90^\circ$  and  $\theta_o=90^\circ$  in the item **I**, where the nucleus rotates about the  $y$  axis and remains triaxial at all  $J_{\text{cal}}$  and the rotational band does not terminate. This result shows that a band termination and its  $J_{\text{cal}}$  value can be sensitive to the  $\theta_o$  value.

In contrast, for **triaxial  $^{24}\text{Mg}$ ,  $\phi_o=90^\circ$ , and  $0^\circ < \theta_o < 90^\circ$ , **CCRM3** predicts a uniform rotation about the  $y$  axis of a triaxial nucleus at all  $J$  values, and the rotational band does not terminate.**

**For triaxial  $^{24}\text{Mg}$ ,  $\phi_o=90^\circ$ , and  $\theta_o=0^\circ$  at**

**$J=2$ , **MSCRM3** predicts  $\langle \hat{J}_1 \rangle = \langle \hat{J}_2 \rangle = 0$**

and a steady uniform rotation of a triaxial nucleus about the  $z$  axis. At  $J_{\text{cal}}=4$  ( $=\Sigma_2 - \Sigma_1 = 20-16$ ), the nucleus becomes axially symmetric about the  $z$  axis and the rotational band terminates.

**For triaxial  $^{24}\text{Mg}$ ,  $\phi_o=90^\circ$ ,  $\theta_o=0^\circ$ ,**

****CCRM3** predicts a similar rotation to that predicted above by **MSCRM3**.**

**For triaxial  $^{24}\text{Mg}$ ,  $\phi_o=89^\circ$ , and**

**$\theta_o=54.7^\circ$  at  $J_{\text{cal}}=2$ , **MSCRM3** predicts that the rotational-state instability**

**(discussed above) reduces  $\langle \hat{J}_1 \rangle$  to near**

zero at the end of the iteration process resulting in a nearly planar triaxial rotation of a triaxial  $^{24}\text{Mg}$  in a plane close to the  $y$ - $z$  plane as seen in Figs. 7, 8, and 9. Figs. 8 and 9 show respectively the values of the angular-momentum components and quadrupole moments at each  $J_{\text{cal}}$  value at the end of the iteration process. A similar triaxial rotation of triaxial  $^{24}\text{Mg}$  is predicted at  $J=4$  as seen in Figs. 8 and 9. At  $J=6$ , the rotation becomes uniform along the  $y$  axis (i.e.,  $\langle \hat{J}_1 \rangle \approx \langle \hat{J}_3 \rangle \approx 0$ ) and  $^{24}\text{Mg}$

remains triaxial, as seen in Figs. 8 and 9. At  $J=8$ ,  $^{24}\text{Mg}$  remains triaxial and the uniform rotation transitions to a triaxial rotation, as seen in Figs. 8 and 9. The **MSCRM3** (and **CCRM3**) equations involve expectations of operators with respect to the cranked wavefunction. Therefore, these equations are non-linear and hence may have oscillatory solutions. This happens in the solutions of **MSCRM3** equations at  $J=6$  and 8. To eliminate these oscillatory solutions and obtain steady converged rotations at  $J=6$  and 8, the input and output values of the variables in each iteration step are linearly mixed and used as input in the next iteration step<sup>15</sup>. The angular momentum and quadrupole moments predicted in this manner are shown in Figs. 10 and 11 (also in Figs. 8 and 9). At  $J_{\text{cal}}=10$  the nuclear rotation and shape become almost axially symmetric about the  $x$  axis, as seen in Figs. 8 and 9. At  $J_{\text{cal}} J=12$  ( $=\Sigma_3 - \Sigma_1 = 28-16=12$ ), the nuclear rotation and shape become

<sup>15</sup> Although the linear-mixing method works well here, a more accurate approach to obtaining

converged solution is to use Broyden's method [104,105,106].

spherically symmetric (as seen in Figs. 8 and 9) and the rotational band terminates.

**Fig. 7: MSCRM3 predicted angular momentum  $\langle J_k \rangle$  versus iteration # for  $\phi_0=89^\circ$  and  $\theta_0=54.7^\circ$  at  $J_{cal}=2$  in triaxial  $^{24}\text{Mg}$**

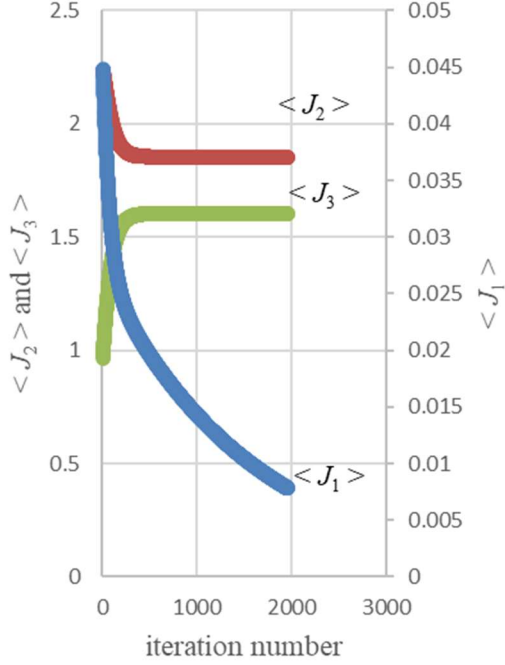


**Fig. 8: MSCRM3 predicted  $\langle J_k \rangle$  versus  $J_{cal}$  at end of iteration process for  $\phi_0=89^\circ$  and  $\theta_0=54.7^\circ$  in triaxial  $^{24}\text{Mg}$**

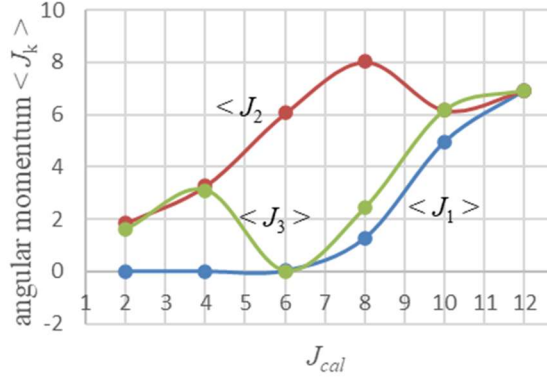


**Fig. 9: MSCRM3 predicted quadrupole moments  $\langle x_k^2 \rangle$  versus  $J_{cal}$  for  $\phi_0=89^\circ$  and  $\theta_0=54.7^\circ$  in triaxial  $^{24}\text{Mg}$**

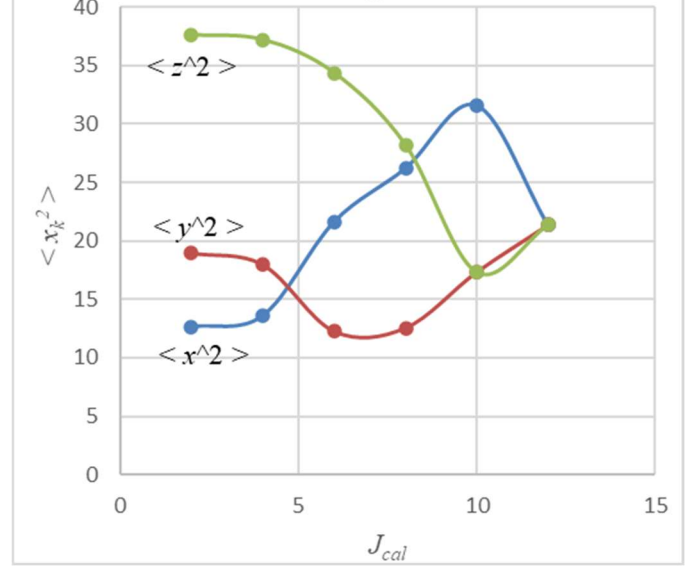


**Fig. 10: MSCRM3 predicted angular momentum  $\langle J_k \rangle$  versus iteration # for  $\phi_0=89^\circ$ ,  $\theta_0=54.7^\circ$ , and  $J_{cal}=8$  in triaxial  $^{24}\text{Mg}$**

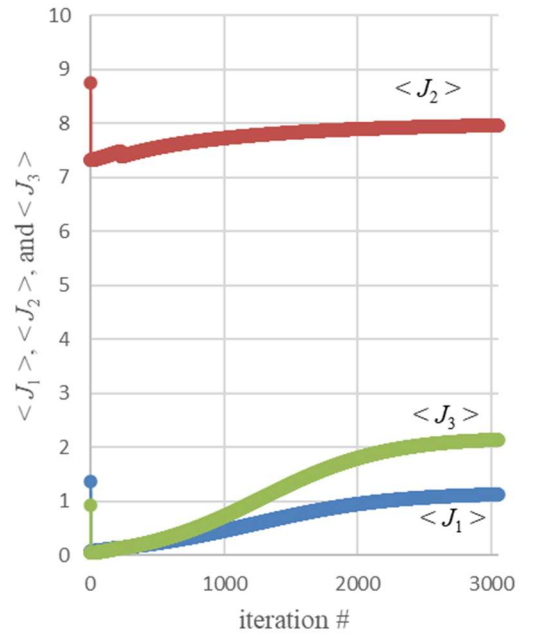
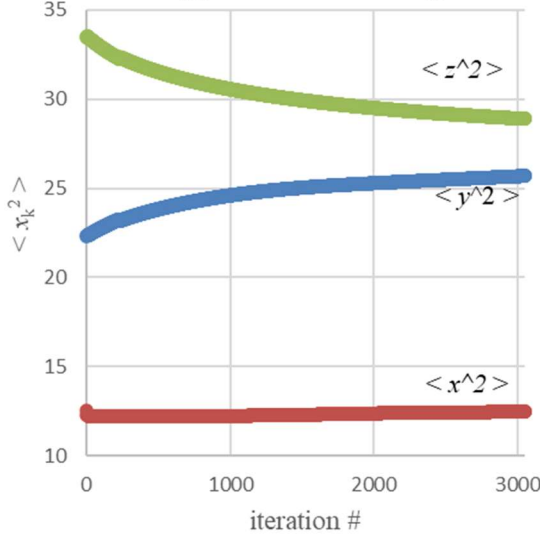


**Fig. 11: MSCRM3 predicted quadrupole moment  $\langle x_k^2 \rangle$  versus iteration # for  $\phi_o=89^\circ$ ,  $\theta_o=54.7^\circ$ , and  $J_{\text{cal}}=8$  in triaxial  $^{24}\text{Mg}$**



For triaxial  $^{24}\text{Mg}$ ,  $0^\circ < \phi_o \leq 89^\circ$  and  $0^\circ < \theta_o < 90^\circ$ , MSCRM3 predicts results similar to those for  $\phi_o=89^\circ$  and  $\theta_o=54.7^\circ$ , except that as  $\theta_o$  approaches  $90^\circ$ , the rotation becomes closer to being uniform along the  $y$  axis.

For triaxial  $^{24}\text{Mg}$ ,  $\phi_o=89^\circ$  and  $\theta_o=90^\circ$   $J_{\text{cal}}=2$ , MSCRM3 predicts a steady rotation about the  $y$  axis with very small values of  $\langle \hat{J}_1 \rangle$  and  $\langle \hat{J}_3 \rangle$ , which begin to slowly increase up to  $J_{\text{cal}}=13$  and 10 respectively (refer to Fig. 12) because of competing effects of the three terms in

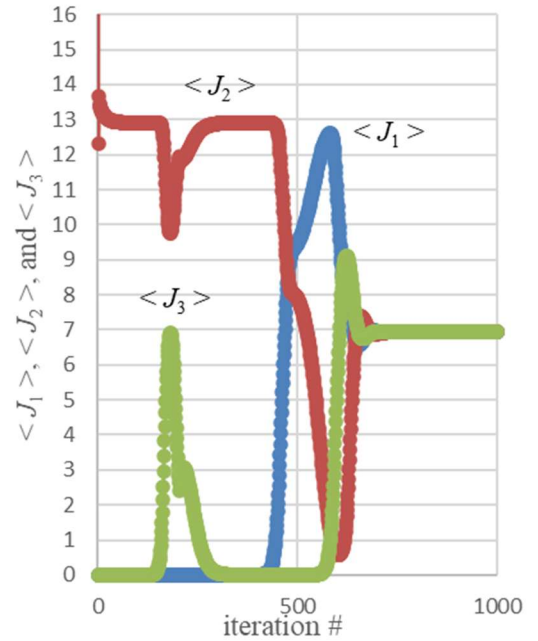
the two sums  $\sum_{k=1}^{k=3} \frac{\partial \alpha_k}{\partial \Omega_1} \cdot \Sigma_k$  and

$\sum_{k=1}^{k=3} \frac{\partial \alpha_k}{\partial \Omega_2} \cdot \Sigma_k$  in Eq. (10). At  $J_{\text{cal}}=12$ ,

$\langle \hat{J}_1 \rangle$  and  $\langle \hat{J}_3 \rangle$  become comparable with  $\langle \hat{J}_2 \rangle$ . Therefore, during the

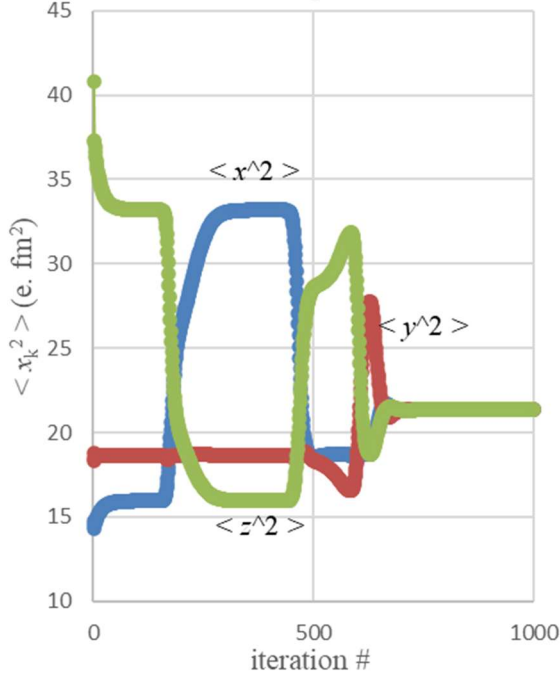
iteration at  $J_{\text{cal}}=12$ , the uniform rotation about the  $y$  axis transitions to a triaxial rotation of a triaxial nucleus (as seen in Figs. 12 and 13) and eventually to a spherically symmetric rotation of a spherical nucleus, at which point the rotational band terminates at  $J_{\text{cal}}=12$  ( $= \Sigma_3 - \Sigma_1 = 28 - 16 = 12$ )<sup>16</sup>.

**Fig. 12: MSCRM3 predicted angular momentum  $\langle J_k \rangle$  and  $J_{\text{cal}}$  versus iteration # for  $\phi_o=89^\circ$ ,  $\theta_o=90^\circ$ , and  $J_{\text{cal}}=12$  in triaxial  $^{24}\text{Mg}$**



<sup>16</sup> The  $J=12$  excitation energy level in  $^{24}\text{Mg}$  is also predicted in an  $sd$ -shell model calculation [111] and observed in an experiment [112].

**Fig. 13: MSCRM3 predicted quadrupole moments  $\langle x_k^2 \rangle$  versus iteration # for  $\phi_o=89^\circ$ ,  $\theta_o=90^\circ$ , and  $J_{cal}=12$  in triaxial  $^{24}\text{Mg}$**



In contrast, for triaxial  $^{24}\text{Mg}$ ,  $\phi_o=89^\circ$ ,  $0^\circ < \theta_o \leq 90^\circ$ , CCRM3 predicts a uniform rotation of triaxial nucleus about the  $x$  axis at  $J=2, 4, 6$ , and  $8$ . At  $J=8$ , the nucleus becomes axially symmetric about the  $x$  axis and the rotational band terminates.

For triaxial  $^{24}\text{Mg}$ ,  $\phi_o=89^\circ$  and  $\theta_o=0^\circ$ , MSCRM3 and CCRM3 predict results that are identical to those for  $\phi_o=90^\circ$  and  $\theta_o=0^\circ$  presented above.

For triaxial  $^{24}\text{Mg}$ ,  $\phi_o=0^\circ$ ,  $0^\circ < \theta_o < 90^\circ$  at  $J_{cal}=2$ , MSCRM3 predicts that  $\langle \hat{J}_2 \rangle$  and  $\langle \hat{J}_3 \rangle$  vanish as a consequence of rotational-state instability, and  $\theta$  increases to  $90^\circ$ , resulting in a uniform rotation about the  $x$  axis at  $J_{cal}=2, 4$ , and

6. At  $J_{cal}=8$ ,  $\langle \hat{J}_1 \rangle$  and  $\langle z^2 \rangle$  begin to decrease (due to the incompressibility condition), and  $\langle \hat{J}_3 \rangle$  and  $\langle y^2 \rangle$  begin to increase (due to centrifugal stretching) (refer to Figs. 14 and 15). These changes cause the uniform rotation about the  $x$  axis to transition to a planar rotation in  $x$ - $z$  plane, and finally to a uniform rotation about the  $z$  axis when  $\langle \hat{J}_1 \rangle$  vanishes at  $J_{cal}=8, 10$  (as seen in Figs. 14 and 15). At  $J_{cal}=11.583$ , after prolonged iterations, the rotation about the  $z$  axis at the start of the iteration transitions to a uniform rotation about the  $45^\circ$  line in the  $x$ - $z$  plane at which point  $\langle \hat{J}_1 \rangle$  begins to increase and the  $\langle \hat{J}_3 \rangle$  begins decrease until they equalize, and  $\langle y^2 \rangle$  increases and  $\langle x^2 \rangle$  decreases until  $\langle x^2 \rangle$  becomes equal to  $\langle z^2 \rangle$  (refer to Figs. 16 and 17). At a higher  $J_{cal}$ , the rotation transitions to a uniform rotation about the  $z$  axis and the nucleus becomes triaxial. This sequential pattern of uniform and planar rotations and axially symmetric and triaxial shapes repeats itself at higher  $J_{cal}$  values. Thus, the rotational band does not terminate.



**Fig. 14: MSCRM3 predicted angular momentum  $\langle J_k \rangle$  versus iteration # for  $\phi_0=0^\circ$  and  $\theta_0=54.7^\circ$  at  $J_{\text{cal}}=8$  in triaxial  $^{24}\text{Mg}$**

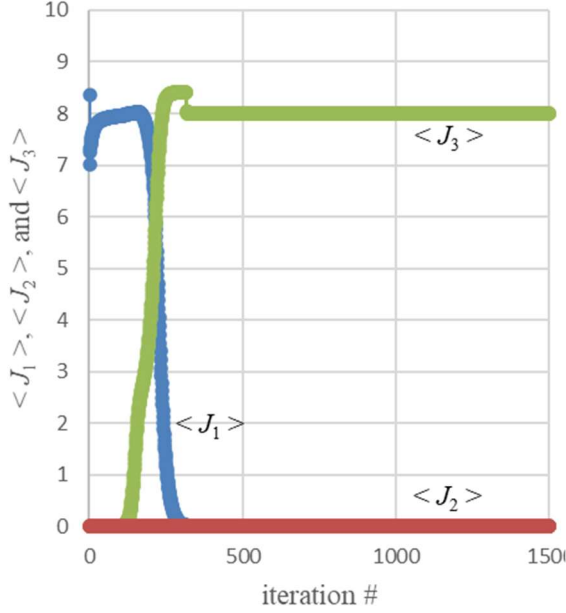
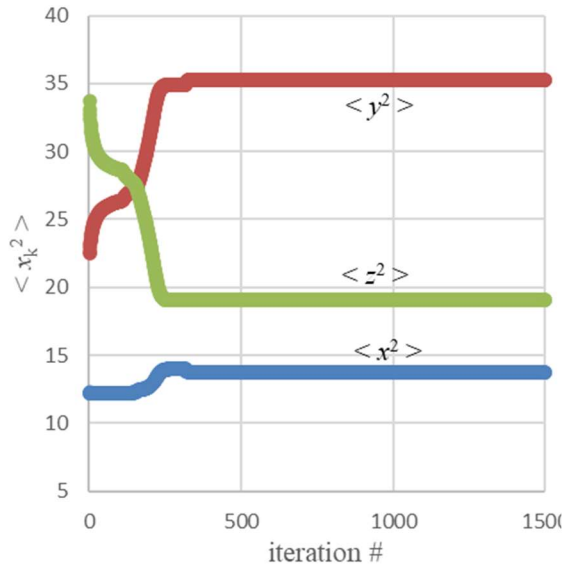
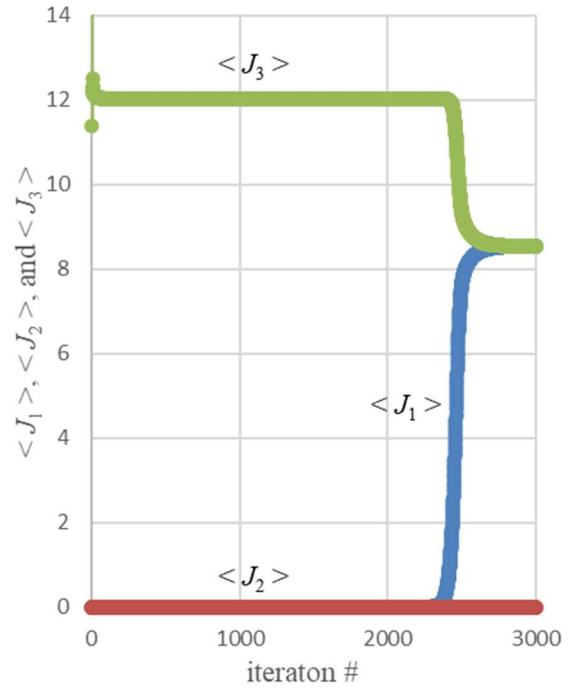


**Fig. 15: MSCRM3 predicted quadrupole moments  $\langle x_k^2 \rangle$  versus iteration # for  $\phi_0=0^\circ$  and  $\theta_0=54.7^\circ$  at  $J_{\text{cal}}=8$  in triaxial  $^{24}\text{Mg}$**



rotation of triaxial nucleus about the  $x$  axis at  $J=2,4,6$ , and  $8$ . At  $J=8$ , the nucleus becomes axially symmetric about the  $x$  axis and the rotational band terminates.

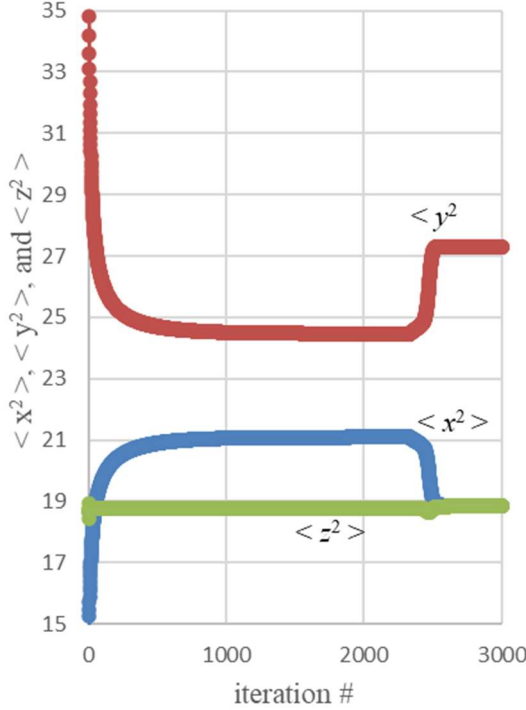
**Fig. 16: MSCRM3 predicted angular momentum  $\langle J_k \rangle$  versus iteration # for  $\phi_0=0^\circ$  and  $\theta_0=54.7^\circ$  at  $J_{\text{cal}}=11.583$  in triaxial  $^{24}\text{Mg}$**



In contrast, for triaxial  $^{24}\text{Mg}$ ,  $\phi_0=0^\circ$ ,  $0^\circ<\theta_0<90^\circ$ , CCRM3 predicts a uniform



**Fig. 17: MSCRM3 predicted quadrupole moments  $\langle x_k^2 \rangle$  versus iteration # for  $\phi_o=0^\circ$  and  $\theta_o=54.7^\circ$  at  $J_{\text{cal}}=11.583$  in triaxial  $^{24}\text{Mg}$**



**For triaxial  $^{24}\text{Mg}$ ,  $\phi_o=0^\circ$  and  $\theta_o=0^\circ$ ,** **MSCRM3** predicts a steady uniform rotation of a triaxial nucleus about the  $z$  axis. At  $J_{\text{cal}}=4$  ( $=\Sigma_2 - \Sigma_1=20-16=4$ ), the nucleus becomes axially symmetric about the  $z$  axis and the rotational band terminates.

**For triaxial  $^{24}\text{Mg}$ ,  $\phi_o=0^\circ$  and  $\theta_o=0^\circ$ ,** **CCRM3** predicts rotations similar to those predicted above by MSCRM3.

**For triaxial  $^{24}\text{Mg}$ ,  $\phi_o=90^\circ$  and  $\theta_o=90^\circ$ ,** **MSCRM3** predicts a uniform steady rotation about the  $y$  axis at  $J_{\text{cal}}=2,4,6,8,10$ , and  $12$ , and higher  $J_{\text{cal}}$  values. The rotational band does not terminate.

**For triaxial  $^{24}\text{Mg}$ ,  $\phi_o=90^\circ$  and  $\theta_o=90^\circ$ ,** the rotation predicted by **CCRM3** is similar to that predicted above by MSCRM3.

**For triaxial  $^{24}\text{Mg}$ ,  $21^\circ \leq \phi_o < 89^\circ$ , and  $\theta_o=90^\circ$ ,** at  $2 \leq J_{\text{cal}} < 12$ , **MSCRM3** predicts a steady uniform rotation about the  $y$  axis of a triaxial nucleus. At  $J_{\text{cal}}=12$  ( $=\Sigma_3 - \Sigma_1=28-16=12$ ), the nucleus and the rotation become spherically symmetric and the rotational band terminates, similarly to that for  $\phi_o=89^\circ$  and  $\theta_o=90^\circ$  at  $J_{\text{cal}}=12$ .

**For triaxial  $^{24}\text{Mg}$ ,  $0^\circ < \phi_o \leq 20^\circ$ , and  $\theta_o=90^\circ$ ,** **MSCRM3** predicts no rotation of any kind at any  $J_{\text{cal}}$ .

In contrast, **for triaxial  $^{24}\text{Mg}$ ,  $0^\circ \leq \phi_o < 90^\circ$ , and  $0^\circ < \theta_o \leq 90^\circ$ ,** **CCRM3** predicts a uniform rotation of triaxial nucleus about the  $x$  axis at  $J=2,4,6$ , and  $8$ . At  $J=8$ , the nucleus becomes axially symmetric about the  $x$  axis and the rotational band terminates.

**For  $\phi_o=90^\circ$ , and  $0^\circ < \theta_o \leq 90^\circ$ ,** **CCRM3** predicts a uniform rotation about the  $y$  axis of a triaxial nucleus at all  $J$  values, and the rotational band does not terminate.

**For triaxial  $^{24}\text{Mg}$ ,  $\phi_o=0^\circ$  and  $\theta_o=90^\circ$ ,** **MSCRM3** predicts a uniform rotation about the  $x$  axis at  $2 \leq J_{\text{cal}} < 8$ . At  $J_{\text{cal}}=8$ , the nucleus becomes axially symmetric about the  $x$  axis and the rotational band terminates.

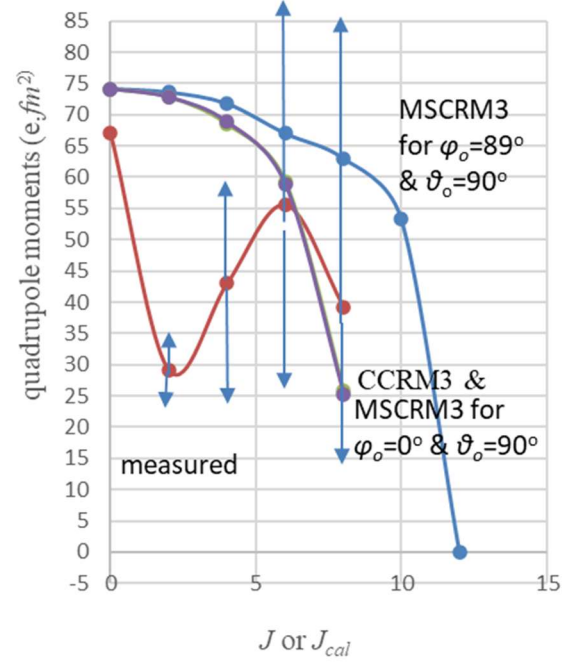
**For triaxial  $^{24}\text{Mg}$ ,  $\phi_o=0^\circ$  and  $\theta_o=90^\circ$ ,** the rotation predicted by **CCRM** is similar to that predicted above by MSCRM3.

Fig. 18 compares the CCRM3 and MSCRM3 predicted and measured quadrupole moment  $Q$  for  $\phi_o = 89^\circ$  and  $\theta_o = 90^\circ$  and  $\phi_o = 0^\circ$  and  $\theta_o = 90^\circ$  in triaxial  $^{24}\text{Mg}$  (note the large uncertainties in the measured  $Q$  [5,109,113])<sup>17</sup>. Fig. 17 shows that MSCRM3 and CCRM3 predict similar  $Q$  for the case  $\phi_o = 0^\circ$  and  $\theta_o = 90^\circ$ , where the rotation is about the  $x$  axis and the band terminates at  $J=8$  when the nucleus becomes axially symmetric. For the case  $\phi_o = 89^\circ$  and  $\theta_o = 90^\circ$ , where the rotation is about the  $y$  axis and the rotational band terminates at  $J=12$  when nucleus and rotation become spherically symmetric, MSCRM predicts a larger  $Q$  because of higher  $J$  value and hence larger centrifugal-induced elongation along the  $z$  axis and smaller constant-volume-condition-induced compression along the  $x$  axis.

Shell-model calculation and experiments [111,112] and the MSCRM3 prediction for  $21^\circ \leq \phi_o \leq 89^\circ$  and  $0^\circ < \theta \leq 90^\circ$  presented above show that the rotational band in  $^{24}\text{Mg}$  extends to  $J=12$ . MSCRM3 predicts that this rotational band terminates at  $J=12$  when the nucleus and rotation about the  $y$  axis become spherically symmetric. In contrast, CCRM3 predicts that the band terminates at  $J=8$  when the nucleus becomes axially symmetric about the  $x$  axis. It seems then that the microscopic angular velocity in MSCRM3 is needed to explain the observed rotational band cut-off at  $J=12$  in  $^{24}\text{Mg}$ .

<sup>17</sup> Note that the main objective in this article is to determine the major difference between CCRM3 and

Fig. 18: Measured and MSCRM3 and CCRM3 predicted quadrupole moments versus  $J$  or  $J_{cal}$  for  $\phi_o = 0^\circ$  and  $\theta_o = 90^\circ$  and  $\phi_o = 89^\circ$  and  $\theta_o = 90^\circ$  in triaxial  $^{24}\text{Mg}$



The above results for  $^{24}\text{Mg}$  indicate that MSCRM3 predicts a broader range of nuclear rotations and shapes and their transitions than does CCRM3.

The above results also show that CCRM3 predicts only uniform principal-axis rotation of a triaxial  $^{24}\text{Mg}$ . This result may not be in conflict with the conclusion in [51,54] that “in even-even nuclei tilted rotations occur if and only if the nucleus has a triaxial shape in its ground state” because [51,54] solved numerically the equations of the deformed-harmonic-oscillator CCRM3 and studied the stability of tilted rotation of nuclei over a range of mass numbers using only one kind of nucleons since [54] was more

MSCRM3 predicted results and not to compare them to measurements.

concerned with determining local and global minima of  $E_{\text{int}}$  in the space of  $(\Omega', \theta', \phi')$  and mass number, and we have found the results to be sensitive to the number of nucleons since it affects the values of  $\Sigma_k$  in Eq. (9).

- J. For triaxial  $^{28}\text{Si}$ , neither MSCRM3 nor CCRM3 predict any physically meaningful rotation in  $^{28}\text{Si}$  for any  $J$  and any values of  $\phi_o$  and  $\theta_o$ .**
- K. For oblate  $^{24}\text{Mg}$  and  $^{28}\text{Si}$ , MSCRM3 and CCRM3 predict no steady stable collective rotation of any kind (single-particle rotations about  $z$  axis is excepted).**

The above predictions of **CCRM3** for

## 5. Summary and conclusions

The Conventional cranking model with its constant free angular-velocity parameter (hence its time reversal and  $D_2$  non-invariances) is frequently used in nuclear structure studies. To investigate the impact of a dynamic (quantum operator) angular velocity on the results of such studies, and hence whether a dynamic angular velocity is needed or not, a quantum microscopic self-consistent, time-reversal, and  $D_2$  and hence signature invariant cranking model Hamiltonian for triaxial rotation (MSCRM3) is derived in two steps. In the first step a quantum microscopic rotor Hamiltonian  $\hat{H}$  is derived by applying a microscopic exponential rotation operator to a deformed nuclear state, which approximately satisfies a nuclear Schrodinger equation (as one obtained from, for example, a Hartree-Fock calculation for an open-shell nuclei).  $\hat{H}$  is

$^{28}\text{Si}$  may not be in conflict with the conclusion in [51,54] that “in even-even nuclei tilted rotations occur if and only if the nucleus has a triaxial shape in its ground state” because [54] solved numerically the equation of the deformed-harmonic-oscillator CCRM3 and studied the stability of tilted rotation of nuclei over a range of mass numbers using only one kind of nucleons since [54] was more concerned with determining local and global minima of  $E_{\text{int}}$  in the space of  $(\Omega', \theta', \phi')$  and mass number, and we have found the results to be sensitive to the number of nucleons since it affects the values of  $\Sigma_k$ .

made to depend on only the square of the angular-momentum operator with no explicit coupling to any intrinsic operators by choosing the rotation angles in the rotation operator to be given by a rigid-flow velocity-field prescription and to be canonically conjugate to the angular momentum. In the second step, Hartree-Fock variational method is applied to  $\hat{H}$  to obtain MSCRM3 Hamiltonian  $\hat{H}_{\text{HFcr}}$  plus residuals of the square of the angular-momentum operator and two-body interaction and other negligibly small correction terms. The MSCRM3 Hamiltonian is identical in form to the conventional cranking model Hamiltonian for triaxial rotation (CCRM3) except that in MSCRM3 the angular velocity is given by the ratio of the expectations of the angular momentum and rigid-flow kinematic

moment of inertia. As a consequence,  $\hat{H}_{HFCr}$  is time-reversal and  $D_2$  invariant, rendering the wavefunction a superposition of either even or odd angular-momentum eigenstates, unlike the case in CCRM3.

For a self-consistent deformed harmonic oscillator (mean-field) potential, the governing MSCRM3 and CCRM3 equations and those of the self-consistency and constant-volume conditions are determined in closed algebraic forms using Feynman's theorem and a closed-form equation for the three normal-mode frequencies of  $\hat{H}_{HFCr}$ . These equations are solved iteratively. The simple deformed harmonic-oscillator potential energy is used to facilitate the comparison of the MSCRM3 and CCRM3 predicted results and the previous CCRM3 predictions that used this potential, and determine the differences between them in a transparent way with a fewest number of adjustable parameters.

A summary of the results obtained from the solutions of MSCRM3 and CCRM3 equations for prolate  $^{20}\text{Ne}$ ,  $^{24}\text{Mg}$ , and  $^{28}\text{Si}$ , and oblate and triaxial  $^{24}\text{Mg}$ , and  $^{28}\text{Si}$  is as follows:

- CCRM3 predicts only a uniform rotation, where the angular momentum and angular velocity are parallel vectors. MSCRM3 generally predicts a wobbling rotation, where the angular velocity and momentum vectors are not parallel.
- CCRM3 and MSCRM3 predict that the self-consistency condition renders the rotational states unstable and causes them to decay to zero angular momentum unless prevented by an angular-momentum constraint (i.e., an

imposition of a desired angular momentum) on the wavefunction as in the conventional cranking model.

- MSCRM3 predicts a rotational relaxation of the intrinsic system in reaction to the imposition and subsequent removal of the condition of a desired angular momentum  $J$ . This relaxation causes the calculated intrinsic angular momentum to be either larger or smaller than  $J$ .
- In CCRM3, the rotational instability mentioned above causes the initial triaxial rotation to transition to a planar uniform rotation in the  $x$ - $y$  plane and subsequently to a uniform rotation about the  $x$  or  $y$  axis with a possible band termination at some higher  $J$ . An exception to this rule is when the initial rotation is axially symmetric, in which case it remains so at all  $J$  values with no band termination. This happens in prolate  $^{20}\text{Ne}$ ,  $^{24}\text{Mg}$ , and  $^{28}\text{Si}$ . Therefore, CCRM3 does not predict any steady stable triaxial rotation in any of the nuclei  $^{20}\text{Ne}$ ,  $^{24}\text{Mg}$ , and  $^{28}\text{Si}$ . These results may not be in conflict with the analysis result in [54], which concluded that "in even-even nuclei tilted rotations occur if and only if the nucleus has a triaxial shape in its ground state" because [54] used only one kind of nucleons and the results are sensitive to the number of nucleons.
- MSCRM3 predicts uniform principal-axis rotation and planar non-uniform (i.e., wobbling) rotation in the  $x$ - $y$  plane for prolate  $^{20}\text{Ne}$ ,  $^{24}\text{Mg}$ , and  $^{28}\text{Si}$ . However, for planar wobbling axially-symmetric (i.e., along the  $45^\circ$  line in the  $x$ - $y$  plane) rotation in  $^{20}\text{Ne}$ , MSCRM3 predicts that at  $J=8$  the rotation transitions to a uniform rotation about the  $x$  axis because of the feedback between the angular velocity and momentum. This transition reduces the energy-level spacing between  $J=6$  and 8

as observed in experiments [5,7]. This result solves the long-known mystery as to the cause of this energy-level spacing reduction. In contrast, CCRM3 does not predict this rotation transition and the resulting energy-level spacing reduction. It is shown that using the residuals of the square of the angular momentum and two-body interaction, and to a lesser extent the spin-orbit interaction in MSCRM3 removes the remaining discrepancy between the predicted and measured excitation energies in  $^{20}\text{Ne}$ .

- MSCRM3 and CCRM3 predict that a rotational band terminates when the nucleus becomes axially symmetric about the uniform-rotation axis at  $J=8, 4$ , and  $12$  in prolate  $^{20}\text{Ne}$ ,  $^{24}\text{Mg}$ , and  $^{28}\text{Si}$  respectively (and also at  $J=8$  in  $^{24}\text{Mg}$ ) at some angular-velocity-vector orientation angles. For triaxial  $^{24}\text{Mg}$ , MSCRM3 predicts a rotational band termination at  $J=4$ , and  $8$  when the nucleus become axially symmetric, and at  $J=12$  when the nucleus becomes spherically symmetric. For triaxial  $^{24}\text{Mg}$ , CCRM3 predicts a band termination at  $J=4$  and  $8$  when the nucleus become axially symmetric. It seems then that the dynamic angular velocity in MSCRM3 is needed to predict the band termination at  $J=12$  in  $^{24}\text{Mg}$  (which is observed in shell-model calculations and experiments [111,112]). At some angular-velocity orientation angles, MSCRM3 predicts no band termination in triaxial  $^{24}\text{Mg}$  whereas CCRM3 does, and vice versa.
- In a number of cases for triaxial  $^{24}\text{Mg}$ , MSCRM3 predicts no rotation of any kind over a range of angular-velocity polar angles whereas CCRM3 does. In a number of cases MSCRM3 predicts

band termination whereas CCRM3 does not and vice versa.

- It is shown that neither MSCRM3 nor CCRM3 predict any physically meaningful rotations in triaxial  $^{28}\text{Si}$  for any values of  $J$  and the angular-velocity orientation angles.
- No steady stable collective rotation of any kind is predicted by either of MSCRM3 and CCRM3 for oblate  $^{24}\text{Mg}$  and  $^{28}\text{Si}$ .
- In the above calculations, oscillatory non-convergent solutions to the non-linear MSCRM3 and CCRM3 equations are eliminated using linear mixing of the values of the input and output variables in each iteration step as input in the next iteration step.
- From the MSCRM3 predicted energy-level spacing reduction for axially-symmetric rotation in  $^{20}\text{Ne}$ , and the significant differences between MSCRM3 and CCRM3 predictions on the types of rotational band and its termination angular momentum and shape deformation, we may conclude that the dynamic angular velocity in MSCRM3 appears to be necessary and a further analysis is recommended.

In future, it may be useful and instructive to study in more detail the differences between the two model predictions for the above and other nuclei and for more realistic interactions (including Nilsson's oscillator, pairing, etc.) to ascertain the impact of the interaction on the predicted rotations in  $^{24}\text{Mg}$  and  $^{28}\text{Si}$ , and to investigate the possibility of other types of rotations. It may also be useful to generalize MSCRM3 to include vibrational excitations.

## Appendix A: Detailed derivation of collective rotor Hamiltonian $\hat{H}$

The transformed rotor Hamiltonian  $\hat{H}$  in Eq. (18) is derived as follows<sup>18</sup>. We apply the rotationally-invariant exponential rotation operator  $e^{i\vec{\theta} \cdot \hat{J}/\hbar}$  to a deformed nuclear state  $|\Phi\rangle$  to obtain the rotated state:

$$|\Phi(\theta_k'')\rangle = e^{i\vec{\theta} \cdot \hat{J}/\hbar} \cdot |\Phi\rangle \equiv e^Z \cdot |\Phi\rangle \quad (\text{A1})$$

The rotationally-invariant rotation operator in Eq. (A1) is similar to that in [96] and transforms the nuclear Hamiltonian  $\hat{H}'_o$  symmetrically in the angular-momentum operator components along the three space-fixed-frame axes, unlike the rotation operator in terms of the Euler angles used in the angular-momentum projection and other studies [4,5,6,13,68,69,71]. The rotational invariance of the rotation operator in Eq. (A1) also eliminates the need to specify the action of the angular-momentum operator on the rotation angles in the transformation of the Hamiltonian  $\hat{H}'_o$  (in contrast to the situation in the uniaxial-rotation case in [arXiv:1810.11836]).

Inserting Eq. (A1) for  $|\Phi_o\rangle$  into the nuclear Schrodinger equation:

$$\begin{aligned} \hat{H}'_o |\Phi_o\rangle &\equiv \left( \sum_{n=1}^A \frac{\hat{p}_n^2}{2M} + \hat{V} \right) |\Phi_o\rangle \\ &= E_J |\Phi_o\rangle, \end{aligned} \quad (\text{A2})$$

we obtain the transformed Schrodinger equation:

$$\begin{aligned} \hat{H} |\Phi(\bar{\theta}'')\rangle &\equiv e^Z \cdot \hat{H}'_o \cdot e^{-Z} \cdot |\Phi(\bar{\theta}'')\rangle \\ &= E_J |\Phi(\bar{\theta}'')\rangle \end{aligned} \quad (\text{A3})$$

where the transformed nuclear Hamiltonian  $\hat{H}$  is given by:

$$\begin{aligned} \hat{H} &\equiv e^Z \cdot \hat{H}'_o \cdot e^{-Z} \\ &= \frac{1}{2M} \sum_{n=1}^A e^Z \cdot \hat{p}_n^2 \cdot e^{-Z} + \hat{V} \end{aligned} \quad (\text{A4})$$

Since  $\bar{\theta}''$  in Eq. (A1) defines the orientation of a deformed nuclear state and this orientation changes from a state to state according to Eq. (A3), we conclude that  $\bar{\theta}''$  should be considered a dynamical variable and is therefore considered to be a function of at least the nucleon co-ordinates.

Therefore, in Eq. (A4),  $\bar{\theta}''$  and  $\hat{p}_n^2$  do not commute. Eq. (A3) shows that each of the rotated wavefunction  $|\Phi(\theta_k'')\rangle$  in Eq. (A1) satisfies Eq. (A3) with the same energy  $E_J$ .

In other words, the Hamiltonian  $\hat{H}$  and  $|\Phi(\theta_k'')\rangle$  for all orientations  $\theta_k''$  describe degenerate (or collapsed) rotational states with the same energy  $E_J$ . Hence, we may conclude that  $\hat{H}$  has an intrinsic character (which is examined further below) and  $|\Phi(\theta_k'')\rangle$  is a superposition of angular-momentum eigenstates. (For the case of the center-of-mass motion, Eq. (A4) becomes:

$\hat{H} = H_o - \frac{1}{2MA} P^2$ , where  $\vec{P}$  is the center-of-mass linear momentum, and hence the correct mass  $MA$  is predicted.) The

<sup>18</sup> We use the space-fixed-frame-axis components of the dynamic rotation angle  $\bar{\theta}$  and angular-momentum operator vectors because they simplify the analysis and provide a transformed  $\hat{H}'_o$  that is a function symmetric in square of the angular momentum components along the space-fixed-frame axes, whereas the usual rotation operator

$e^{i\alpha \cdot \hat{J}_3/\hbar} \cdot e^{i\beta \cdot \hat{J}_2/\hbar} \cdot e^{i\gamma \cdot \hat{J}_1/\hbar}$  in terms of the Euler angles along body-fixed-frame axes and the corresponding operator  $e^{i\theta_1 \cdot \hat{J}_1/\hbar} \cdot e^{i\theta_2 \cdot \hat{J}_2/\hbar} \cdot e^{i\theta_3 \cdot \hat{J}_3/\hbar}$  along the space-fixed axes obtained from the Euler rotation operator have complicated transformation properties and yield an  $\hat{H}'_o$  that is complicated asymmetric function of the angular momentum components.

transformed Hamiltonian  $\hat{H}$  in Eq. (A4) is observed to be rotationally invariant since:

$$\begin{aligned} \left[ \hat{J}, e^Z \cdot \hat{p}_n^2 \cdot e^{-Z} \right] &= e^Z \left[ \hat{J}, \hat{p}_n^2 \right] e^{-Z} = 0, \\ \left[ \hat{J}, \hat{V} \right] &= 0 \end{aligned} \quad (\text{A5})$$

The invariance in Eq. (A5) is one of the major advantages of the rotation operator  $e^Z$  over other forms of the rotation operator such as the successive Euler rotation operators used in the literature.

We evaluate  $e^Z \cdot \hat{p}_n^2 \cdot e^{-Z}$  in Eq. (A4) using the following expansion in powers of  $Z$ :

$$\begin{aligned} e^Z \cdot \hat{p}_n^2 \cdot e^{-Z} &= \hat{p}_n^2 + \left[ Z, \hat{p}_n^2 \right] \\ &+ \frac{1}{2!} \left[ Z, \left[ Z, \hat{p}_n^2 \right] \right] + \dots \end{aligned}$$

(A6)

Using the rotational invariance of  $Z$  and  $\hat{p}_n^2$  in Eq. (A5), we can easily evaluate the terms in Eq. (A6) and show that the terms in powers of  $Z$  higher than two vanish since  $\vec{\theta}''$  is chosen to be a function of only the nucleon co-ordinates. Inserting these results into Eq. (A4), we obtain:

$$\begin{aligned} \hat{H} &= \hat{H}'_o + \frac{i\hbar}{2M} \cdot \sum_{n=1}^A \sum_{k=1}^3 \nabla_n^2 \theta_k'' \cdot \hat{J}_k \\ &- \frac{1}{M} \cdot \sum_{n=1}^A \sum_{k=1}^3 \left( \vec{\nabla}_n \theta_k'' \cdot \vec{p}_n \right) \cdot \hat{J}_k \\ &+ \frac{1}{2M} \cdot \sum_{n=1}^A \sum_{k=1}^3 \vec{\nabla}_n \theta_k'' \cdot \vec{\nabla}_n \theta_l'' \cdot \hat{J}_k \cdot \hat{J}_l \end{aligned} \quad (\text{A7})$$

To eliminate all couplings between  $\vec{J}$  and intrinsic (such as shear) operators in the third term on the right-hand-side of Eq. (A7) arising from the  $\vec{p}_n$  term, we use, as in [arXiv:1810.11836], the following rigid-flow velocity-field prescription for the rotation angles  $\vec{\theta}''$ :

$$\begin{aligned} \frac{\partial \theta_1''}{\partial x_{nj}} &= - \sum_{k=2}^3 {}_1\chi_{jk} x_{nk} \\ {}_1\chi_{jk} &= -{}_1\chi_{kj} = 0 \text{ for } j, k \neq 2, 3 \end{aligned} \quad (\text{A8})$$

$$\begin{aligned} \frac{\partial \theta_2''}{\partial x_{nj}} &= - \sum_{k=1, \neq 2}^3 {}_2\chi_{jk} x_{nk} \\ {}_2\chi_{jk} &= -{}_2\chi_{kj} = 0 \text{ for } j, k \neq 1, 3 \end{aligned} \quad (\text{A9})$$

$$\begin{aligned} \frac{\partial \theta_3''}{\partial x_{nj}} &= - \sum_{k=1}^2 {}_3\chi_{jk} x_{nk} \\ {}_3\chi_{jk} &= -{}_3\chi_{kj} = 0 \text{ for } j, k \neq 1, 2 \end{aligned} \quad (\text{A10})$$

where each  ${}_k\chi$  is a real  $3 \times 3$  anti-symmetric matrix. Each of the selections in Eqs. (A8), (A9), and (A10) picks the collective rigid-flow component of the velocity field of each nucleon rendering the third term on the right-hand-side of Eq. (A7)

to depend only on  $\vec{J}^2$ . The non-zero elements of each  ${}_k\chi$  in Eqs. (A8), (A9), and (A10) are determined by choosing  $\theta_k''$  and  $\hat{J}_l$  to be a canonically conjugate pair, i.e.,

$$\left[ \theta_k'', \hat{J}_l \right] = i\hbar \delta_{kl} \quad (\text{A11})$$

Inserting Eqs. (A8), (A9), and (A10) into Eq. (A11), we obtain:

$${}_1\chi_{kl} = \frac{1}{\hat{\mathcal{G}}_1}, \quad {}_2\chi_{kl} = -\frac{1}{\hat{\mathcal{G}}_2}, \quad {}_3\chi_{kl} = \frac{1}{\hat{\mathcal{G}}_3} \quad (\text{A12})$$

$$\begin{aligned} \hat{\mathcal{G}}_1 &\equiv \sum_{n=1}^A (y_n^2 + z_n^2), \\ \hat{\mathcal{G}}_2 &\equiv \sum_{n=1}^A (x_n^2 + z_n^2), \\ \hat{\mathcal{G}}_3 &\equiv \sum_{n=1}^A (x_n^2 + y_n^2) \end{aligned} \quad (\text{A13})$$

where  $M\hat{\mathcal{G}}_k$  is the  $k^{\text{th}}$  principal-axis component of the kinematic rigid-flow moment of inertia tensor<sup>19</sup>. We observe that, for the choice in Eqs. (A8), (A9), (A10),

<sup>19</sup> Note that the rigid-flow prescription for  $\theta_k''$  in Eqs. (A8), (A9), (A10), and (A12) is a collective analogue of the Birbrair's single-particle  $\theta_n$  [97]:

$\vec{\nabla}_n \theta_n = \vec{e}_x \times \vec{r}_n / (y_n^2 + z_n^2)$ , where  $\vec{e}_x$  is a unit vector along the  $x$  axis.  $\theta_n$  has continuous second-order

(A12), and (A13), we obtain the result:

$$[\theta_k, \hat{J}_l] = i\hbar \frac{Q_{kl}}{\hat{\mathcal{G}}_k} \approx 0 \quad (k \neq l) \quad (\text{A14})$$

since  $Q_{lk}$  for  $k \neq l$  is very small compared to

$\hat{\mathcal{G}}_k$ , where  $Q_{lk} \equiv \sum_{n=1}^A x_{nl} \cdot x_{nk}$  is the  $kl^{th}$

component of the quadrupole moment tensor. (However, there is no need to know the action of  $\hat{J}_l$  on  $\theta_k$  for  $k \neq l$  in any derivations of the equations in this article.) Inserting Eqs. (A8), (A9), (A10), (A12), and (A13) into Eq. (A7), we obtain:

$$\begin{aligned} \hat{H} \equiv \hat{H}'_o - \sum_{k=1}^3 \frac{1}{2M\hat{\mathcal{G}}_k} \cdot \hat{J}_k^2 \\ - \sum_{k \neq l=1}^3 \frac{Q_{lk}}{2M\hat{\mathcal{G}}_l\hat{\mathcal{G}}_k} \cdot \hat{J}_l \cdot \hat{J}_k \end{aligned} \quad (\text{A15})$$

We observe that the second term on the right-hand side of Eq. (A15) resembles the rotational kinetic energy of a rotating triaxial classical rigid body [98] with the exception that all the operators in Eq. (A15) are space-

fixed-frame (and not body-fixed) axis components. The third term in Eq. (A15) is negligibly small because  $M^2\hat{\mathcal{G}}_l\hat{\mathcal{G}}_k$  is very large and the off-diagonal elements  $MQ_{lk}$  of the quadrupole-moment tensor are small, and hence the third term in Eq. (A15) can be and is neglected.

Inserting Eq. (A15) into Eq. (A3) and neglecting the last term in Eq. (A15), we obtain the following Schrodinger equation for a triaxial rotation of a microscopic quantum ideal triaxial rotor:

$$\begin{aligned} \hat{H} \left| \Phi(\vec{\theta}'') \right\rangle \\ \equiv \left[ \hat{H}'_o - \sum_{k=1}^3 \frac{\hat{J}_k^2}{2M\hat{\mathcal{G}}_k} \right] \left| \Phi(\vec{\theta}'') \right\rangle \quad (\text{A16}) \\ = E_J \left| \Phi(\vec{\theta}'') \right\rangle \end{aligned}$$

## References

- [1] M. Bouten, M.C. Bouten, and E. Caurier, Nucl. Phys. A193, 49 (1972).
- [2] J.D. Rogers, Ann. Rev. Nucl. Sci. 15, 241 (1965).
- [3] J.M. Eisenberg and W. Greiner, *Nuclear Theory* (North Holland, Amsterdam, 1970).
- [4] A. deShalit and H. Feshbach, *Theoretical Nuclear Physics* (John Wiley & Sons, Inc., N.Y., 1974), Vol. 1.
- [5] A. Bohr and B.R. Mottelson, *Nuclear Structure* (Benjamin, N.Y., 1975), Vol. II.

---

mixed derivatives (i.e.,  $\vec{\nabla}_n \times \vec{\nabla}_n \theta_n = 0$ ) in any spatial region that excludes the  $x$  axis along which  $\theta_n$  is singular. Whereas  $\theta_k''$  has discontinuous second-order mixed derivatives (i.e.,  $\vec{\nabla}_n \times \vec{\nabla}_n \theta_k \neq 0$ ). The difference in the discontinuity between  $\vec{\nabla}_n \theta_k''$  and  $\vec{\nabla}_n \theta_n$  arises because of the many-body nature of  $(\hat{\mathcal{G}}_k)^{-1}$  in Eq. (A12). However, the discontinuity in  $\vec{\nabla}_n \theta_k''$  is small because the expectation of  $\hat{\mathcal{G}}_k$  is a large number. On the other hand, for a rigid-body

motion  $\vec{\nabla}_n \theta_{rig} = \omega_{rig} \vec{e}_x \times \vec{r}_n$ , with a constant angular velocity  $\omega_{rig}$ ,  $\vec{\nabla}_n \theta_{rig}$  is inherently discontinuous. Nevertheless,  $\theta_{rig}$  is commonly used in the analysis of a rigid-body motion [97] with impunity because the second mixed derivatives of  $\theta_{rig}$  do not appear in any of the analysis equations. Similarly, the discontinuity  $\vec{\nabla}_n \times \vec{\nabla}_n \theta_k'' \neq 0$  is of no consequence in the derivation of MSCRM3 in this article because the second-order mixed derivatives of  $\theta_k''$  do not appear anywhere in the derivation of the equations in this article.



- [6] P. Ring and P. Schuck, *The Nuclear Many-Body Problem* (Springer-Verlag, N.Y., 1980).
- [7] S.G. Nilsson and I. Ragnarsson, *Shapes and shells in nuclear structure* (Cambridge University Press, Cambridge, UK. 1995).
- [8] A. Faessler, W. Greiner, and R.K. Sheline, Nucl. Phys. 70, 33 (1965).
- [9] A. Faessler, W. Greiner, and R.K. Sheline, Nucl. Phys. 80, 417 (1965).
- [10] J.P. Davidson, Rev. Mod. Phys. 37 (1965) 105.
- [11] G. Gneuss and W. Greiner, Nucl. Phys. A171, 449 (1971).
- [12] A.F. Stamp, Nucl. Phys. 164, 81 (1971).
- [13] H.J. Mang, Physics Report 18, no. 6, 325 (1975).
- [14] G. Ripka, J.P. Blaizot, and N. Kassis, in *Heavy-Ion, High-Spin States and Nuclear Structure*, Trieste Int. Seminar on Nuclear Physics, September 17-December 21, 1973 (IAEA, Vienna, 1975).
- [15] A. Bohr, Rev. Mod. Phys. 48, 365 (1976).
- [16] R.M. Lieder and H. Ryde. in *Advances in nuclear physics*, edited by M. Baranger and E. Vogt. Plenum Press, New York. 1978) Vol. 10.
- [17] S. Cwiok, J. Dudek, and Z. Szymanski, Phys. Letts. 76B, 263 (1978).
- [18] B. Grammaticos and K.F. Liu, Il. Nuovo Cimento, 50, 349 (1979).
- [19] R. Bengtsson and S. Frauendorf, Nucl. Phys. A 314, 27 (1979).
- [20] J. Fleckner, U. Mosel, P. Ring, and H.-J. Mang, Nucl. Phys. A331, 288 (1979).
- [21] M. Diebel, D. Glas, U. Mosel, and H. Chandra, Nucl. Phys. A333, 253 (1980).
- [22] A.L. Goodman, G.S. Goldhaber, A. Klein, and R.A. Sorensen, Nucl. Phys. A347 (1980).
- [23] T. Troudet and R. Arvieu, Ann. Phys. 134, 1 (1981).
- [24] A. Faessler, in Proc of Conf. on High Angular Momentum Properties of Nuclei, Proc. Oak Ridge, Tennessee, November 2-4, 1982, edited by N.R. Johnson, Hardwood Academic Publishers N.Y. 1982, Vol. 4.
- [25] F.S. Stephens, in *Frontiers in nuclear dynamics*, edited by R.A. Broglia and C.H. Daso, Plenum Press, New York. 1985.
- [26] J. Kvasil and R.G. Nazmitdinov, Nucl. Phys. A439, 86 (1985).
- [27] J. Kvasil and R.G. Nazmitdinov, Sov. J. Part. Nucl. 17, 265 (1988).
- [28] P. Ring, Progr. Part. Nucl. Phys. 73, 193 (1996).
- [29] T. Tanaka, F. Sakata, T. Marumori, and K. Iwasawa. Phys. Rev. C 56, 180 (1997).
- [30] S. Frauendorf, Rev. Mod. Phys. 73, 463 (2001).
- [31] R.G. Nazmitdinov, D. Almehed, F. Donau, Phys. Rev. C 65, 041307 (2002).
- [32] M. Matsuzaki, Y.R. Shimizu, and K. Matsuyanagi, Phys. Rev. C 65, 034325 (2004).
- [33] M.A. Deleplanque, S. Frauendorf, V.V. Pashkevich, S.Y. Chu, and A. Unzhakova, Phys. Rev. C 69, 044309 (2004).
- [34] J. Kvasil and R.G. Nazmitdinov, Phys. Rev. C69, 031304 (2004).

- [35] J. Kvasil and R.G. Nazmitdinov, Phys. Rev. C 73, 014312 (2006).
- [36] J. Kvasil and R.G. Nazmitdinov, J. Exp. Theor. Phys. Letts. 83, 187 (2006).
- [37] J. Kvasil and R.G. Nazmitdinov, Phys. Letts. B 650, 331 (2007).
- [38] J. Kvasil, R.G. Nazmitdinov, A.S. Sitdikov, and P. Vesely, Phys. of Atomic Nuclei 70, 1386 (2007).
- [39] R.G. Nazmitdinov and J. Kvasil, J. Exp. Theor. Phys. 105, 962 (2007).
- [40] E.R. Marshalek, Nucl. Phys. A 331, 429 (1979).
- [41] J.G. Valatin, Proc. Roy. Soc. (London) 238, 132 (1956).
- [42] P. Gulshani and A. B. Volkov, J. Phys. G: Nucl. Phys. 6, 1335 (1980).
- [43] A.V. Afanasjev, in *Handbook of Nuclear Physics*, edited by I. Tanihata, H. Toki, and T. Kajino (Springer, Singapore, 2022).
- [44] M.L. Cescato, Y. Sun, and P. Ring, Nucl. Phys. A 533, 455 (1991).
- [45] M.G. Vassanji and M. Harvey, Nucl. Phys. A 344, 61 (1980).
- [46] F. Cuypers, Nucl. Phys. A 468, 237 (1987).
- [47] H. Frisk and R. Bengtsson, Phys. Letts. B 196, 14 (1987).
- [48] S. Frauendorf, Nucl. Phys. A 557, 259c (1993).
- [49] A.F. Dodaro and A.L. Goodman, Nucl. Phys. A 596, 91 (1995).
- [50] T. Horibata and N. Onishi, Nucl. Phys. A 596, 251 (1996).
- [51] W.D. Heiss and R.G. Nazmitdinov, Phys. Letts. B 397, 1 (1997).
- [52] S. Frauendorf, Nucl. Phys. A 677, 115 (2000).
- [53] V. I. Dimitrov, S. Frauendorf, and F. Döna, Phys. Rev. Lett. 84, 5732 (2000).
- [54] W.D. Heiss and R.G. Nazmitdinov, Phys. Rev. C 65, 054304 (2002).
- [55] I. Hamamoto, Phys. Rev. C 65, 044305-1 (2002).
- [56] M. Matsuzaki, Y.R. Shimizu, and K. Matsuyanagi, Phys. Rev. C 65, 041303(R)-1 (2002).
- [57] M. Oi and P.M. Walker, Phys. Letts. B 576, 75 (2003).
- [58] P. A. Olivius and R. Bengtsson, Phys. Rev. C 69, 014310, 2004.
- [59] M. Matsuzaki and S-I. Ohtsubo, Phys. Rev. C 69, 064317-1 (2004).
- [60] M. Matsuzaki, Y.R. Shimizu, and K. Matsuyanagi, Phys. Rev. C 69, 034325-1 (2004).
- [61] D.J. Thouless and J.G. Valatin, Nucl. Phys. 31, 211 (1962).
- [62] F. Villars and G. Cooper, Ann. Phys. (N.Y.) 56, 224 (1970).
- [63] T.H.R. Skyrme, Proc. Roy. Soc. (London) A 70, 433 (1957).
- [64] D.J. Thouless and R.E. Peierls, Nucl. Phys. 38, 154 (1962).
- [65] R.A. Sorensen, Rev. Mod. Phys. 45, 353 (1973).
- [66] D.J. Thouless, Nucl. Phys. 21, 225 (1960).
- [67] D. R. Inglis, Phys. Rev. 103, 1786 (1956).
- [68] R.E. Peierls and J. Yoccoz, Proc. Phys. Soc. 70, 381 (1957).
- [69] F.M.H. Villars, Nucl. Phys. 74, 353 (1965).
- [70] Chi-Yu Hu, Nucl. Phys. 66, 449 (1965).

- [71] E.B. Bal'butsev and I.N. Mikhailov, Akad. Nauk. SSSR, Izv. Ser. Fiz. 30, 1170 (1966).
- [72] E.R. Marshalek and J. Weneser, Ann. Phys. 53, 564 (1969).
- [73] F. Villars and N. Schmeing-Rogerson, Ann. Phys. 63 (1971) 443.
- [74] B.L. Birbrair, Nucl. Phys. A257, 445 (1976).
- [75] J. Pelet and J. Letourneux, Nucl. Phys. A281, 277 (1977).
- [76] I.N. Mikhailov and D. Janssen, Izvestiya Akademii Nauk SSSR, Seriya Fizicheskaya, 41, 35 (1977).
- [77] I.N. Mikhailov and D. Jansen, Phys. Letts. 72B, 303 (1978).
- [78] D. Janssen, I.N. Mikhailov, R.G. Nazmitdinov, B. Nerlo-Pomorska, K. Pomorska, and R.Kh. Safarov, Phys. Letts. 79B, 347 (1978).
- [79] B.L. Birbrair, Sov. J. Nucl. Phys. 28, 631 (1979).
- [80] A.V. Ignatyuk and I.N. Mikhailov, Sov. J. Nucl. Phys. 30, 343 (1979).
- [81] A. Klein, and M. G. Vassanji, Nucl. Phys. A317, 116 (1979).
- [82] D. Janssen and I.N. Mikhailov, Nucl. Phys. A318, 390 (1979).
- [83] J. Sau, J. Phys. A: Math. Gen. 12, 1971 (1979).
- [84] K. Goeke and P.-G. Reinhard, Ann. Phys. 124, 249 (1980).
- [85] A.K. Kerman and N. Onishi, Nucl. Phys. A361, 179 (1981).
- [86] N. Onishi, Nucl. Phys. A456, 279 (1986).
- [87] A.K. Klein, Phys. Rev. C 63, 014316 (2000).
- [88] P. Gulshani, Nucl. Phys. A 832, 18 (2010).
- [89] V. G. Zelevinsky, Supplement of Prog. Theor. Phys. 74 & 75 (1983).
- [90] R.P. Feynman, Phys. Rev. 56, 340 (1939).
- [91] M.J.A. de Voigt, J. Dudek, and Z. Szymanski, Rev. Mod. Phys. 55, 949 (1983).
- [92] P. Ring and A. V. Afanasjev, Acta Physica Polonica B, 32 (2001).
- [93] P. Olbratowski, J. Dobaczewski, J. Dudek, Phys. Rev. C 73, 054308 (2006).
- [94] Y. Shi, C. L. Zhang, I. Dobaczewski, and W. Nazarewicz, Phys. Rev. C 88, 034311 (2013).
- [95] J-P. Blaizot and G. Ripka, *Quantum Theory of Finite System* (MIT Press, Cambridge, Massachusetts, U.S.A., 1986).
- [96] M.E. Rose, *Elementary Theory of Angular Momentum*, (John Wiley & Sons, Inc., N.Y., 1974).
- [97] B.L. Birbrair, Phys. Letts. 72B (1978) 425.
- [98] H. Goldstein, *Classical Mechanics* (Addison-Wesley Publishing Co., Inc, Reading, Massachusetts, USA. 1950).
- [99] P. Gulshani, J. Phys. A: Math. Gen. 14, 97 (1981).
- [100] C.A. Levinson, Phys. Rev. 132, 2184 (1963).
- [101] I. Kelson and C.A. Levinson, Phys. Rev. 134, B269 (1964).
- [102] M.K. Banerjee, D. D'Oliveira, and G.J. Stephenson, Jr., Phys. Rev. 181, 1404 (1969).
- [103] J.P. Elliott and J.A. Evans, Nucl. Phys. A324 (1979) 12.
- [104] C.G. Broyden, Math. Comput 19, 577 (1965).
- [105] D.D. Johnson, Phys. Rev. B38, 128807 (1988).
- [106] A. Baran, A. Bulgac, M.M. Forbes, C. Hagen, W. Nazarewicz, N. Schunck, and

- M.V. Stoitsov, Phys. Rev. C78, 01438 (2008).
- [107] G. Ripka, in *Fundamentals in Nuclear Theory*, Lectures presented at Int. Course, Triesta, October 03-December 16, 1966, Editors: A. DeShalit and C. Villi (IAEA, Vienna, 1967).
- [108] J. Zofka and G. Ripka, Nucl. Phys. A168, 65 (1971).
- [109] Y. Abgrall, B. Morand, and E. Caurier, Nucl. Phys. A192, 372 (1972).
- [110] Y. Abgrall, G. Baron, E. Caurier, and G. Monsonego, Nucl. Phys. A131, 609 (1969).
- [111] A.A. Al-Sammarraie, S. Fadhill, and H.A. Kassim, Armenian Journal of Physics 8, 170 (2015).
- [112] E.S. Diffenderfer, et. al., Physical Review C 85, 034311(2012).
- [113] D. Branford, A.C. McGough, and I.F. Wright, Nucl. Phys. A241, 349 (1975).